~~Assessment~~Investigation of ice cloud modelling capabilities for the irregularly shaped Voronoi ice scattering models in climate simulations ~~with CAM5~~

Ming Li[1], Husi Letu[1], Yiran Peng[3], Hiroshi Ishimoto[4], Yanluan Lin[3], Takashi Y. Nakajima[2], Anthony Baran[5,6], Zengyuan Guo[3,7], Yonghui Lei[2], Jiancheng Shi[8]

[1]Aerospace Information Research Institute, Chinese Academy of Sciences, Beijing 100010, China
[2]Research and Information Center (TRIC), Tokai University, 4-1-1 Kitakaname Hiratsuka, Kanagawa 259-1292, Japan
[3]Ministry of Education Key Laboratory for Earth System Modeling, Department of Earth System Science, Tsinghua University, Beijing 10084, China
[4]Meteorological Research Institute, Japan Meteorological Agency (JMA), Nagamine 1-1, Tsukuba 305-0052, Japan
[5]Met Office, Fitzroy Road, Exeter EX1 3PB, UK
[6]School of Physics, Astronomy and Mathematics, University of Hertfordshire, Hatfield, AL10 9AB, UK
[7] Laboratory for Climate Studies, National Climate Center, China Meteorological Administration, Beijing 100081, China
[8]National Space Science Center, Chinese Academy of Sciences, Beijing 100190, China

Correspondence to: Husi Letu (husiletuw@hotmail.com~~husiletu@radi.ac.cn~~)

Abstract.

Both weather/climate models and ice cloud remote sensing applications all need to obtain effective ice crystal scattering (ICS) properties and the parameterization scheme.~~Climate models and satellite remote sensing applications require accurate descriptions of ice cloud optical and radiative properties through parameterization of their scattering properties. While abundant irregularly shaped ice particle habits present a challenge for modelling ice clouds.~~ An irregularly shaped Voronoi ICS model ~~ice particle habit (Voronoi model)~~ has been ~~developed and recently~~ suggested to be effective in remote sensing applications for several satellite programs, e.g., Himawari-8, GCOM-C (Global Change Observation Mission-Climate) and EarthCARE (Earth Cloud Aerosol and Radiation Explorer).~~inferring the microphysical and radiative properties of ice clouds from Himawari-8 and GCOM-C satellite measurements.~~ As ~~a~~ continuation ~~of previous~~ work ~~by~~ of Letu et al. (2016), an ice cloud optical property parameterization scheme (Voronoi scheme) of the Voronoi ICS model is employed in the Community Integrated Earth System Model (CIESM) to simulate the optical and radiative properties of ice clouds. We utilized the single-scattering properties (extinction efficiency, single-scattering albedo and asymmetry factor) of the Voronoi model from the ultraviolet to the infrared, combined with 14,408 particle size distributions obtained from aircraft measurements to complete the Voronoi scheme. The Voronoi scheme and existing schemes (Fu, Mitchell, Yi and Baum-yang05) are applied

to the CIESM to simulate 10-yr global cloud radiative effects during 2001-2010. Simulated global-averaged cloud radiative forcing at the top of the atmosphere (TOA) for Voronoi and other four existing schemes are compared to the Clouds and the Earth's Radiant Energy System Energy Balanced And Filled (EBAF) product. The results show that the difference in shortwave and longwave global-averaged cloud radiative forcing at the TOA between the Voronoi scheme simulations and EBAF products is 1.1% and 1.4%, which is lower than that of the other four schemes. Particularly for regions (from 30°S to 30°N) where ice clouds occur frequently, the Voronoi scheme provides the closest match with EBAF products compared with other four existing schemes. The results in this study fully demonstrated the effectiveness of the Voronoi ICS model in the simulation of the radiative properties of ice clouds in the climate model.~~in this study, we develop a broadband ice cloud scheme based on the Voronoi model through parameterization for use in the Community Atmosphere Model, Version 5 (CAM5). With single scattering properties of Voronoi model, ice cloud bulk scattering properties are integrate over particle size distributions of 11 field campaigns and are parameterized over particle effective diameter. The new ice cloud scheme is compared with four ice cloud schemes (the Yi, Mitchell, Baum-yang and Fu scheme), and is evaluated through the General circulation model version of the Rapid Radiative Transfer Model (RRTMG), and simulations of the top of atmosphere (TOA) shortwave and longwave cloud forcing (SWCF and LWCF) in CAM5. The Clouds and the Earth's Radiant Energy System (CERES) satellite data was selected as validation data. Results indicated that the Voronoi scheme can minimize differences between the satellite-based measurements and CAM5 simulations of global TOA SWCF compared to other four schemes, but performance is not significant for TOA LWCF. For tropical ice clouds, Voronoi scheme has advantages of ice cloud modelling capabilities for shortwave (SW) and longwave (LW) spectrum over other four schemes. In general, it is found that the Voronoi model has advantages over conventional ice cloud schemes and is sufficient for ice cloud modelling in climate simulations with CAM5.~~

1 Introduction

Ice clouds cover about 20% - 30% of the global area (Rossow and Schiffer, 1991; Wang et al., 1996; Stubenrauch et al., 2013), and they strongly affect the earth's energy budget and climate system mainly due to their optical and radiative properties (Liou, 1986, 1992; Baran, 2012; Ramaswamy and Ramanathan, 1989). The radiative properties of ice clouds

mainly depend on their optical properties (e.g., scattering albedo and optical thickness), which are significantly influenced by the microphysical properties (e.g., ice particle sizes and habits) of ice clouds (Baran, 2009; Yang et al., 2015; Yang et al., 2018). Based on the accurate knowledge of ice particle sizes and habits, the single-scattering properties (e.g., extinction efficiency, single-scattering albedo and asymmetry factor) of ice particles can be calculated by using the light scattering computational method to develop the ice crystal scattering (ICS) model/database. Combined with the single-scattering properties of the ICS model/database and size distributions, the optical properties of ice clouds can be simulated through the parameterization scheme, and the radiative properties of ice clouds can be further simulated based on the radiative transfer theory.

At present, satellite remote sensing and weather/climate models are two effective ways to understand the ice cloud optical and radiative properties through the ice cloud optical property parameterization scheme in radiative transfer models. However, numerous field observations (Rossow and Schiffer, 1999; Lawson et al., 2006; Heymsfield et al., 2017; Lawson et al., 2019), e.g., the First International Satellite Cloud Climatology Project (ISCCP) Regional Experiments (FIRE-I) in 1986 and 1991 (Rossow and Schiffer, 1999) and the European cirrus experiment in 1989 (Liou, 1992) have shown that ice clouds contain a large variety of non-spherical ice particle sizes and habits, which can lead to inaccurate simulations of the optical and radiative properties of ice clouds in nature. Our understanding of how ice particle habits affect the optical and radiative properties of ice clouds is still limited (Heymsfield and Miloshevich, 2003; van Diedenhoven et al., 2014b; van Diedenhoven, 2018). The current insufficient knowledge of the ice cloud microphysical properties and the ice particle single-scattering properties contributes to inadequate representation of the optical properties in the parameterization scheme, which can directly lead to uncertainties in the simulated radiative properties of ice clouds (Zhang et al., 2015; Yang et al., 2015, 2018; Yi et al., 2017; van Diedenhoven and Cairns, 2020). Thus, the accurate representation of the microphysical properties of ice clouds and ice particle single-scattering properties is essential for the parameterization of ice cloud optical properties and studying the radiative properties of ice clouds in both satellite remote sensing and weather/climate models.

In terms of current light scattering computational methods, it is still difficult for one specific method to accurately calculate the single-scattering properties for non-spherical particles with different size parameter (SZP), which is defined as the ratio of the equivalent-volume sphere's circumference dimension (or π times particle maximum diameters) to the

incident wavelength (Nakajima et al., 2009; Baran, 2012; Yang et al., 2015). The existing light scattering computational methods for non-spherical particles can be generally divided into the approximation method (AM) based on the ray-tracing techniques (Wendling et al., 1979), and the numerical simulation (NM) method based on the approximate solutions of Maxwell equations. The AM method is suitable for non-spherical particles with very large SZPs. The geometrical optics approximation (GOA) method is a typical AM method. This method can capture the halo phenomenon of large hexagonal ice particles in the visible wavelength. However, the AM method is difficult to accurately simulate the single-scattering properties for particles with small and moderate SZPs. The NM method is suitable for particles with small SZPs and can be divided into the volume and surface-based methods depending on how Maxwell equations are solved. The volume-based NM method includes the finite-difference time domain (FDTD) (Yee, 1966; Yang and Liou, 1996b) and discrete dipole-approximation (DDA) methods (Draine and Flatau, 1994; Yurkin and Hoekstra, 2007). A typical method of the surface-based method is the T-matrix method (Havemann and Baran, 2001; Mishchenko and Travis, 1998). However, the NM method requires discretization of the whole volume/surface of the scatterer and needs rather high computational demands (Nakajima et al., 2009), so it is difficult to efficiently calculate the single-scattering properties for particles with moderate and large SZPs. Later, the invariant imbedding T-matrix (II-TM) (Bi et al., 2013a; Bi and Yang, 2014) and physical-geometric optics hybrid (PGOH) method (Bi et al., 2011) are developed for particles with small to moderate SZPs. Combined with the advantages of the AM and NM methods, several improved GOA methods including the geometric optics integral equation (GOIE) (Yang and Liou, 1996; Ishimoto et al., 2012a) and improved geometric-optics method (IGOM) (Yang and Liou, 1995, 1996a; Bi et al., 2010) have been developed. The GOIE and IGOM methods are useful for particles with moderate SZPs, and therefore they can bridge the gap between the AM and NM methods. Thus, the light scattering computation of particles with different SZPs can be completed by a combination of the AM and NM methods.

With the development of the ICS model/database, numerous parameterization schemes of the ice cloud optical properties have been developed for use in the ice cloud remote sensing and weather/climate model applications (Yang et al., 2015, 2018). In terms of weather/climate model applications, Fu (1996) developed a parameterization scheme (referred to as the Fu scheme hereafter) using the GOA-based ICS database for the randomly oriented hexagonal particle (Takano and Liou, 1989). The Fu scheme was subsequently applied to the Fu-Liou radiative transfer model for use in the climate models (Fu,

1996, 2007). Mitchell et al. (1996b, 2006) used the modified anomalous diffraction approximation (MADA) method (Mitchell and Arnott, 1994) to generate an ICS database for a habit mixture and completed a parameterization scheme (referred to as the Mitchell scheme hereafter) combined with the bimodal size distributions (Mitchell et al., 1996a). The Mitchell scheme was then employed in the National Center for Atmospheric Research Community Atmosphere Model (CAM). Yang et al. (2000a) used the IGOM and FDTD methods to develop an ICS database for six ice particle habits. However, this database contains several inconsistencies in the spectral regions caused by differences of particle habits and computational methods. Later, Yang et al. (2013a) utilized the Amsterdam DDA (Yurkin et al., 2007; Yurkin and Hoekstra, 2011a), T-matrix (Mishchenko et al., 1996) and improved IGOM (Bi et al., 2009) methods to generate a spectrally consistent ICS database for 11 ice particle habits. Yi et al. (2013) employed the ICS database of Yang et al. (2013a) and developed a parameterization scheme (referred to as the Yi scheme hereafter) for use in the CAM. For ice cloud remote sensing applications, Baum et al. (2005a, 2005b) used the ICS database of Yang et al. (2000a) to develop a parameterization scheme (referred to as the Baum-yang05 scheme hereafter) for the MODIS collection 5 ice cloud product. C.-Labonnote et al. (2000, 2001) and Doutriaux-Boucher et al. (2000) developed an ICS database for the Inhomogeneous Hexagonal Monocrystal (IHM) containing embedded inclusions (air bubbles and aerosols) and developed a parameterization scheme for use in the ice cloud retrievals from the French satellite Polarization and Directionality of the Earth's Reflectance (POLDER) measurements (Deschamps et al., 1994). Ishimoto et al., (2012) and Letu et al. (2016) developed an ICS database by using a combination method of the FDTD, GOIE and GOM for an irregularly shaped Voronoi model based on in situ microphysical measurements. Letu et al. (2016, 2020) demonstrated that the Voronoi model can effectively retrieve the ice cloud microphysical properties from satellite measurements. Furthermore, the Voronoi model has been adopted for generating official ice cloud products for the Second Generation gLobal Imager (SGLI)/Global Change Observation Mission-Climate (GCOM-C) (Letu et al., 2012, 2016; Nakajima et al., 2019), AHI/Himawari-8 (Letu et al., 2018) and the Multi-Spectral Imager (MSI)/Earth Cloud Aerosol and Radiation Explorer (EarthCARE) satellite programs (Illingworth et al., 2015), which will be launched in 2023. These studies demonstrated the superiority of the Voronoi model in the ice cloud remote sensing applications. However, the performance of the Voronoi model in climate model simulations has not been investigated quantitatively.

Motivated by the abovementioned situations, this study aims to quantify the effects of the Voronoi model on the optical and radiative properties of ice clouds in a climate model in comparison with other ice cloud optical property schemes (Fu, Mitchell, Yi and Baum-yang05). To achieve this goal, we develop an ice cloud optical property parameterization scheme (referred to as the Voronoi scheme hereafter) for the Voronoi model. The Voronoi scheme and other schemes are employed in the Community Integrated Earth System Model (CIESM) (Lin et al., 2020) to simulate shortwave and longwave fluxes at the top of the atmosphere (TOA). The CIESM-based simulations from five schemes are compared with the Earth's Radiant Energy System (CERES) Energy Balanced And Filled (EBAF) products. This study addresses the following questions through the comparison. How different is the Voronoi scheme from other schemes? How, and to what extent does the Voronoi scheme affect the radiative effects of ice clouds? What are the possible reasons for the impacts of the Voronoi scheme?~~The role of ice clouds is very important for Earth-atmosphere energy balance determination through parameterization in remote sensing applications and climate models. A number of field observations, such as the First International Satellite Cloud Climatology Project (ISCCP) Regional Experiment (FIRE-I) from October-November 1986, have shown that ice clouds contain a large variety of particle habits, sizes and complexities (Liou, 1992), as also shown by the following observational studies~~ (Heymsfield et al., 2017; Yang et al., 2018; Lawson et al., 2019)~~. Substantial studies have shown that ice cloud parameterization scheme uncertainties are mainly related to ice particle habits, sizes and microphysical properties, which can lead to substantial radiative discrepancies between satellite measurements and climate model simulations (Zhang et al., 2005). Optimal choice of representative ice particle habit is still difficult to determine.~~

~~The single-scattering properties of the ice particle models and ice cloud parameterization are important for remote sensing applications and climate model simulations of ice cloud radiative properties. The ice cloud parameterization accuracy is mainly determined by the single-scattering properties of the ice particle models. Furthermore, the single-scattering properties of the ice particle model mainly depend on the assumption of ice particle habits and the light-scattering numerical calculation methods. Early studies assumed ice particles to be spherical models, and their single-scattering properties can be accurately determined by the Lorenz-Mie theory~~ (Hulst, 1957)~~. These models were found to be inadequate approximations for the treatment of ice clouds because many aircraft observation measurements have shown that ice clouds are mainly composed of the nonspherical ice particles~~ (Macke et al., 1996; Heymsfield et al., 2002; Heymsfield et al., 2013)~~. In the last few decades,~~

a series of light-scattering computational methods have been developed, including the conventional geometric-optics method (CGOM) (Cai and Liou, 1982), the improved geometric-optics method (IGOM) (Yang and Liou, 1995, 1996a; Bi et al., 2011), the finite-difference time-domain (FDTD) method (Yang and Liou, 1996b), pseudo-spectral time-domain (PSTD) method (Liu, 1997; Chen et al., 2008), discrete-dipole-approximation (DDA) method (Draine and Flatau, 1994; Yurkin and Hoekstra, 2007), the T-matrix method (Macke et al., 1995; Havemann and Baran, 2001) along with the invariant imbedding T-matrix (II-TM) method (Bi et al., 2013a; Bi et al., 2013b; Bi and Yang, 2014), and the boundary element method has been more recently applied to complex ice particle shapes without approximating the geometry of the particle (Groth et al., 2015). With these computational techniques, the research community has made significant progress towards calculating single-scattering properties (namely, the extinction efficiency, asymmetry factor, single-scattering albedo, and complete phase matrix) of nonspherical ice particles. For example, the single-scattering properties of seven ice particle habits at wavelengths from 3 to 100 μm have been computed (Yang et al., 2005) using FDTD (Yang and Liou, 1996b; Sun et al., 1999) and IGOM (Yang and Liou, 1996a). The disadvantages of the data libraries developed by (Yang et al., 2005) are several inconsistencies in the spectral region caused by differences of particle habits and computational methodologies. A spectrally consistent database including 11 ice particle habits at wavelengths from 0.2 to 100 μm, were published by (Yang et al., 2013b) based on a composite method of the Amsterdam discrete dipole approximation (ADDA) (Yurkin and Hoekstra, 2007, 2011b), the T-matrix (Yang et al., 2007; Bi et al., 2013a, 2013bMishchenko et al., 1996) and the IGOM method including the edge effect (Baran and Havemann, 1999). Furthermore, features including air bubbles or aerosol, various habit ensembles, and surface roughness were added into ice particles. For example, randomly oriented hexagonal ice particles containing spherical air bubbles (inhomogeneous hexagonal monocrystals) (IHMs) (Labonnote et al., 2001) were developed for use in the ice cloud parameter retrievals from the French satellite Polarization and Directionality of the Earth's Reflectances (POLDER) measurements (Deschamps et al., 1994). An ensemble ice particle model made of hexagonal column ice particles, was developed by (Baran and Labonnote, 2007; Baran et al., 2014b) for cirrus.

With the developments of light scattering computations, increasing ice cloud parameterization schemes have been developed for ice cloud remote sensing application and climate model simulations based on above ice scattering models. Fu (1996) established an ice cloud parameterization (named Fu hereafter) based on the hexagonal ice particle to the four-stream

approximation of the Fu-Liou radiative transfer models (Fu et al., 1998; Fu, 2007). Baum et al. (2005b) form a new parameterization scheme (named Baum-yang hereafter) based on nine ice particle habits from a library of Yang et al. (2013b) and applied it to the development of ice cloud products in MODIS Collection 5. Yi et al. (2013) developed a parameterization (named Yi hereafter) based on a general habit mixture model that includes nine pristine habits of varying roughness (Yang et al., 2013b). Baran et al. (2014a) presented a new coupled cloud physics-radiation parameterization and implemented it into the Met Office Unified Model Global Atmosphere 5.0 (GA5) configuration based on the optical properties developed by (Baran et al., 2014b). Baran et al. (2016) developed an improved ice cloud optical property parameterization between the model prognostic variable ice water content (IWC) and the environmental temperature. This parameterization is now implemented in the Met Office's latest Earth System model, which is described in (Walters et al., 2019)). In the Community Earth System Model version 1.2.1 (CESM1.2.1) developed by the USA National Center for Atmospheric Research (NCAR) (Hurrell et al., 2013), the atmosphere component model is the Community Atmosphere Model version 5 (CAM5) (Neale et al., 2010). In CAM5, the ice cloud parameterization scheme developed by (Mitchell et al., 1996a; Mitchell et al., 1996b) (named Mitchell hereafter) is utilized for ice cloud optical and radiative properties. Habits of ice particles used for the Mitchell scheme are hexagonal, irregular ice particles, quasi-spherical and 3-D bullet rosettes calculated from the modified anomalous diffraction approximation (MADA) (Mitchell et al., 2006). Based on CESM1.2.1 (Hurrell et al., 2013), the Community Integrated Earth System Model (CIESM) was developed by Tsinghua University (Lin Y L, 2020). CAM5 in CIESM was modified with several new schemes, but it still uses the Mitchell scheme for ice cloud properties. Different ice cloud parameterization can result in significant differences in radiative properties. Ice particle habits is one of the most important influencing factors of ice cloud radiative properties. Zhao et al. (2018) compared three ice cloud parameterizations in CAM5, and their results showed that the difference of downward longwave flux can cause the changes of overall temperature by around 3°C. Yi et al. (2013) found that the effects of ice particle surface roughness on the global shortwave (SW) and longwave (LW) cloud radiative effects (CRE) can reach 1-2 W/m^2 and 0.37 W/m^2, respectively.

The optimal choice of ice particle habit is needed to develop the ice cloud parameterization scheme as accurately as possible and is also significant for cloud-aerosol interactions (Liu et al., 2019; Yan and Wang, 2020). Microphysical measurements showed that a high proportion of irregularly shaped ice particles generated in convective clouds due to collision and

aggregation process (Heymsfield et al., 2002). An irregularly shaped Voronoi model was developed by (Ishimoto et al., 2012) based upon in situ microphysical measurements. Letu et al. (2016) compared five representative ice particle models using the spherical albedo difference (SAD) method, and the results indicated that the irregularly shaped Voronoi model has advantages over the conventional general habitat mixture (GHM) (Baum et al., 2011), IHMs (Labonnote et al., 2001), 5-plate aggregate (Baum et al., 2005a; Baum et al., 2011), apart from the ensemble ice particle model (Baran and Labonnote, 2007), which gave similar results to the Voronoi model. To date, Voronoi model has been adopted in remote sensing studies of official ice cloud products for the Second Generation Global Imager (SGLI)/Global Change Observation Mission-Climate (GCOM-C) (Letu et al., 2012; Letu et al., 2016; Nakajima et al., 2019), the AHI/Himawari-8 (Letu et al., 2018) and Multi-Spectral Imager (MSI)/Earth Cloud Aerosol and Radiation Explorer (EarthCARE) satellite programs (Illingworth et al., 2015), which will be launched in 2023 and has proven to be efficient in the remote sensing retrieval of ice cloud products (Letu et al., 2020). To build on the work of (Letu et al., 2016), this study aims to develop an ice cloud parameterization scheme (named Voronoi hereafter) based on the single-scattering properties of the Voronoi model and evaluate it through atmospheric global climate model CAM5 AGCM simulations of the CIESM. This study focuses on reducing uncertainties in ice cloud radiative properties and studies the influence of irregularly shaped ice particle habits on cloud radiative properties.

This paper is organized as follows. Sections 2 and 3 introduce the data and methodology used in this study, section 4 demonstrates the influence of the Voronoi model on the cloud radiative properties through the radiative transfer model and climate model. Section 5 presents the summary and conclusion of this study.

The current work is presented as follows. Sections 2 and 3 introduce the data and methodology used in this study. Section 4 demonstrates the influence of the Voronoi model on the cloud radiative properties through radiative transfer model and CAM5AGCM multiyear simulations. Section 5 presents the summary and conclusion of this study.

2 Data

2.1 Single-scattering property database for the Voronoi model

~~**2 Single-scattering properties of the Voronoi model database**~~

In this study, the single-scattering property database ~~properties~~ of the Voronoi model~~,~~ developed by Ishimoto et al. (2012) and Letu et al. (2016) ~~(Ishimoto et al., 2012; Letu et al., 2016)~~ is used in the parameterization process.~~, are utilized in the ice cloud parameterization.~~ The single-scattering properties including the extinction efficiency, single-scattering albedo, and asymmetry factor of the Voronoi model from the ultraviolet to the infrared are utilized to calculate the shortwave and longwave optical properties of ice clouds. The single-scattering properties of the Voronoi model are calculated by combination methods of FDTD, GOIE and GOM. This combination method implements a well treatment of particle edge effects (Ishimoto et al., 2012). With this treatment, the gaps between the results calculated by the FDTD and those by the GOIE are relatively small, which can lead to consistence in the single-scattering properties of ice particles. Figure 1 (a) and (b) show the extinction efficiency, single-scattering albedo, and asymmetry factor for Voronoi models that vary with SZPs at wavelengths of 0.64 and 2.21 μm, respectively. Note that the FDTD and GOIE methods are used for small (SZP < 40) and moderate (SZP < 300) ice particles, respectively, and the GOM method is used for large (SZP > 300) particles. The extinction efficiency at wavelengths of 0.64 μm and 2.21 μm has a peak value when the SZP approximately equals to 10 and decreases to be a constant value of 2 with increasing SZPs larger than 100. The single-scattering albedo at both wavelengths is close to 1, which is related to the high values of the imaginary part in the refractive index. The asymmetry factor decreases with the increasing SZPs at the wavelength of 0.64 μm. At the wavelength of 2.21 μm, the asymmetry factor increases for the SZPs smaller than 10 and larger than 300.

2.2 Aircraft-based measurements of the particle size distributions

To generate the parameterization scheme of ice cloud optical properties for application in the climate model simulations, particle size distributions (PSDs) of the Voronoi model need to be assumed in ice clouds. In this study, we utilized 14,408 PSDs derived from in situ aircraft-based measurements obtained in 11 field campaigns (available http://stc-se.com/data/bbaum/Ice_Models/microphysical_data.html) (Heymsfield et al., 2013). These data confirm that the particle

phase is unambiguously ice after filtering by cloud temperature (T≤-40°C). For the fitting of PSDs for the Voronoi model, we adopt the gamma distribution form as follows:

$$n(L) = N_0 L^{\mu} e^{-\lambda L} \quad (1)$$

where L is the particle maximum dimension, $n(L)$ is the particle concentration per unit volume (e.g., 1/cm^3), N_0 is the intercept, λ is the slope, and μ is the dispersion. The physical meaning of the PSD is that $n(L)$ times dL is the number of particles per unit area.

As shown in Figure 2, the particle concentration decreases with increasing L for all ranges. When the temperature is between -60 ℃ and -55 ℃ temperature, the particle concentration is the largest, and it decreases most sharply with increasing L. When the temperature is between -45 ℃ and -40 ℃, as well as between -65 ℃ and -70 ℃ temperature, the particle concentration is the smallest, and it decreases slowly with increasing L.

2.3 Satellite data used in the validation

To evaluate the cloud radiative effects for different schemes of the ICS model, we adopted the CERES EBAF Ed4.1 products (available https://ceres.larc.nasa.gov/data/) (Draine and Flatau, 1994; Doelling et al., 2016) from 2001 to 2010 as validation data. The "toa_cre_sw_mon" and "toa_cre_lw_mon" EBAF products are used to compared with the simulated shortwave and longwave cloud radiative effects from all five schemes. The "toa_cre_sw_mon" and "toa_cre_lw_mon" products are monthly mean shortwave and longwave cloud radiative effects at the TOA, and they are calculated as all-sky fluxes minus total region clear-sky fluxes for shortwave and longwave spectrum. The "toa_sw_all_mon" and "toa_lw_all_mon" EBAF products are monthly mean all-sky outgoing shortwave and longwave fluxes at the TOA, and they are used to compare with simulated upwelling shortwave flux at the TOA (FSUTOA) and upwelling longwave flux at the TOA (FLUTOA) from all schemes. The "sfc_sw_down_all_mon" and "sfc_lw_down_all_mon" are monthly mean all-sky downwelling shortwave and longwave fluxes at the surface, and they are used to compare with simulated downwelling shortwave flux at the surface (FSDS) and downwelling shortwave flux at the surface (FLDS) from all schemes. The spatial and temporal resolution of EBAF data is 1°×1° latitude by longitude and monthly means.

~~The wavelength range is from 0.2 μm to 15 μm, and the particle maximum dimensions (L) of ice particles ranges from approximately 0.5 μm to 716 μm. The single-scattering properties utilized in this study mainly include the extinction~~

~~efficiency (Q_{ext}), single-scattering albedo (*SSA*), absorption efficiency (Q_a), asymmetry factor (g) and the scattering phase function. The refractive indices of this ice crystal habit are derived from the newest library provided by (Warren and Brandt, 2008). The database of single-scattering properties were calculated using a composite approach combining FDTD, geometric optics integral equation (GOIE) (Yang and Liou, 1996a) and GOM methods (Macke et al., 1996). Figure 1 shows the single-scattering properties of ice particles that vary with different size parameters (*SZPs*) at a fixed wavelength of 0.64 μm (Figure 1 a1-a3) and 2.21 μm (Figure 1 b1-b3), respectively. The *SZP* is positively correlated with L and negatively correlated with wavelength, which is shown by equation (1). Note that the FDTD and GOIE methods are used for small (SZP < 40) and moderate particles (SZP < 300), and the GOM method is used for larger particles (SZP > 300). By treating well particle edge effects (Ishimoto et al., 2012), scattering efficiency calculated by a combination of FDTD, GOIE and GOM method is coherent. The extinction efficiency at both wavelengths of 0.64 μm (Figure 1 a1) and 2.21 μm (Figure 1 b1) has a peak value when the *SZP* is equal to 10 and tends to be a constant value of 2 with an increasing *SZP* larger than 100. The minimum extinction efficiency tends to 0 with a decreasing *SZP* smaller than 10 at a wavelength of 2.21μm. The scattering efficiency at both wavelengths of 0.64 μm (Figure 1 a2) and 2.21 μm (Figure 1 b2) is highstrong, and thus, the absorption efficiency is weak, which is related to the imaginary value in the refractive index. The asymmetry factor tends to decrease with increasing *SZP* at a wavelength of 0.64μm (Figure 1 a3). At a wavelength of 2.21μm (Figure 1 b3), there is an increasing asymmetry factor for the *SZP*s smaller than 10 and larger than 300, leading to an increasing proportion of forward scattering.~~

~~$$SZP = \frac{\pi L}{\lambda}, \quad (1)$$~~

3 Methodology

The main flowchart of this study is described in Figure ~~2~~3. Firstly, we developed the parameterization scheme of the Voronoi ICS model by using the aforementioned single-scattering properties of the Voronoi ICS database and large amounts of PSDs. Then, the Voronoi scheme and the other four existing schemes (Fu, Mitchell, Yi and Baum-yang05) were evaluated through simulations of shortwave upward/downward flux profiles in the Rapid Radiative Transfer Model for General circulation model version (RRTMG). The RRTMG was utilized to understand how the different optical properties of the five schemes influence the upward/downward fluxes under several idealized conditions. Furthermore, all schemes were applied

to the CIESM to simulate global shortwave and longwave cloud radiative forcing at the TOA from 2000 to 2010, among which the first year was removed for reaching the equilibrium state and the last ten years were evaluated by EBAF products. The CIESM was employed to evaluate the effectiveness of the Voronoi ICS model in the simulations of ice cloud radiative properties compared with the other four schemes in the climate system.~~Aircraft field campaigns from (Heymsfield et al., 2013) are used to determine particle size distributions (PSDs) in the form of the gamma distribution (Mitchell et al., 1996a) (see equation (2)). Based on the single-scattering properties of the Voronoi model and PSDs, the effective diameter (D_e) (see equation (7)) and the spectral bulk scattering properties of ice clouds, including spectral mass-averaged extinction coefficients (m^2/g) ($K_{ext}(\lambda)$) (see equation (8)), spectral single-scattering albedo ($\varpi(\lambda)$) (see equation (9)) and spectral asymmetry factor ($g(\lambda)$) (see equation (10)) are calculated for all PSDs. Then, band-averaged bulk scattering properties (see equation (11-13)) are integrated over band intervals appropriate in the General circulation model version of the Rapid Radiative Transfer Model (RRTMG) (Clough et al., 2005; Morcrette et al., 2008) and CAM5. For the SW bands, the solar constant is utilized from the solar spectrum ($S(\lambda)$) provided by (Chance and Kurucz, 2010). For the LWlongwave bands, $S(\lambda)$ is replaced with the Planck function. Then, the coefficients of the polynomial expressions of the ice cloud bulk scattering properties as functions of D_e are determined in each band to develop Voronoi scheme for shortwave and longwaveSW and LW spectrum. To assess the ice cloud modeling capabilities of Voronoi scheme, four typical ice cloud schemes (Details are in section 1), including the Fu (Fu et al., 1998), Baum-yang (Baum et al., 2005b), Yi (Yi et al., 2013) and Mitchell scheme (Mitchell et al., 1996a; Mitchell et al., 1996b), are introduced for comparisons through RRTMG and CAM5 simulations. Relevant coefficients in the fitting of extinction coefficients, single-scattering albedo and asymmetry factor for above four schemes can be found in their cited literature. The Clouds and the Earth's Radiant Energy System (CERES) satellite level 3 CERES_SYN1deg_Ed4A products (name SYN1deg hereafter) (Draine and Flatau, 1994; Doelling et al., 2016) is considered to be efficient in many studies (Yi et al., 2013; Zhao et al., 2018). We utilize SYN1deg 1° monthly observed TOA fluxes to validate the cloud radiative properties simulated by five schemes from the CAM5.~~

3.1 Parameterization of ice cloud optical properties

To better understand the ice cloud modelling capabilities of the Voronoi model in climate model~~the CAM5~~ and explain how ice clouds play a role in the climate system, it is necessary to introduce the main scattering parameters to evaluate the Voronoi ICS model ~~ice particle model~~ through the parameterization scheme ~~ice cloud parameterization~~.

The main radiative transfer processes can be simply attributed to extinction, scattering and absorption coefficients (Liou, 1986, 1992), which are calculated by Eq. (2).

$$\beta_{e,s,a} = \int_{L_{min}}^{L_{max}} \sigma_{e,s,a} n(L) dL \quad (2)$$

where $\beta_{e,s,a}$ is the extinction, scattering and absorption coefficients and σ is the cross section (See Table 1 for a list of acronyms). The single-scattering albedo and co-albedo can be defined as the ratio of the scattering and absorption coefficients to the extinction coefficient in the form of Eq. (3).

$$\varpi = \frac{\beta_s}{\beta_e}, \text{ or } 1 - \varpi = \frac{\beta_a}{\beta_e} \quad (3)$$

where ϖ and $1 - \varpi$ are single-scattering albedo and co-albedo, respectively. Based on the extinction coefficient, the optical depth can be defined by Eq. (4).

$$\tau = \int_{z}^{\infty} \beta_e \, dz \quad (4)$$

where τ is the optical depth, z is the outer boundary of the atmosphere. In the assumption of plane-parallel atmospheres, changes in the diffuse intensity penetrating from below the layer considering multiple scattering processes can be given by Eq. (5).

$$I(\tau;\mu;\phi) = \frac{\varpi}{4\pi}\int_0^{2\pi}\int_{-1}^{1} I(\tau;\mu';\phi') P(\mu,\phi;\mu',\phi') d\mu' d\phi' + \frac{\varpi}{4\pi} F_\theta P(\mu,\phi;-\mu_0,\phi_0) e^{-\tau/\mu_0} + (1-\varpi) B[T(\tau)] \quad (5)$$

where P is the phase function corresponding to a volume of ice particles. P (μ, φ; μ', φ') denotes the redirection of the incoming intensity defined by (μ', φ') to the outgoing intensity defined by (μ, φ). I indicate the total (direct plus diffuse) radiance, B indicates Planck's function associated with thermal emissions, and Θ is the scattering angle. Therefore, the

extinction coefficients, single-scattering albedo and phase function are fundamental driving parameters within the transfer of diffuse intensity.

Based on these principles, in this study, we completed the Voronoi scheme by using the single-scattering properties of the Voronoi model and 14,408 groups of PSDs data. The parameterization of the ice cloud optical properties for Voronoi scheme are developed following Eq. (6)-(15). Firstly, the spectral ice cloud optical properties (mass-averaged extinction coefficients, single-scattering albedo and asymmetry factor) for the Voronoi scheme are calculated for all PSDs given by Eq. (6)-(9).

$$D_e = \frac{3}{2}\frac{\int_{L_{min}}^{L_{max}} V(L)n(L)dL}{\int_{L_{max}}^{L_{max}} A(L)n(L)dL} \quad (6)$$

$$K_{ext}(\lambda) = \frac{\int_{L_{min}}^{L_{max}} Q_{ext}(\lambda, L)A(L)n(L)dL}{\rho_{ice}\int_{L_{min}}^{L_{max}} V(L)n(L)dL} \quad (7)$$

$$\varpi(\lambda) = \frac{\int_{L_{min}}^{L_{max}} Q_{sca}(\lambda, L)A(L)n(L)dL}{\int_{L_{min}}^{L_{max}} Q_{ext}(\lambda, L)A(L)n(L)dL} \quad (8)$$

$$g(\lambda) = \frac{\int_{L_{min}}^{L_{max}} g(\lambda, L)\sigma_{sca}(\lambda, L)n(L)dL}{\int_{L_{min}}^{L_{max}} \sigma_{sca}(L)n(L)dL} \quad (9)$$

where D_e is the effective particle diameter, V and A are volume and projected area of Voronoi models. $K_{ext}(\lambda)$ are spectral mass-averaged extinction coefficients (m^2/g), $\varpi(\lambda)$ is spectral single-scattering albedo and $g(\lambda)$ is spectral asymmetry factor. Q_{ext}, g and Q_{sca} are extinction efficiency, asymmetry factor and scattering efficiency for Voronoi models.

Then, based on the spectral bulk optical properties including $K_{ext}(\lambda)$, $\varpi(\lambda)$, and $g(\lambda)$ of ice clouds, the band-averaged optical properties are calculated to apply the parameterization scheme in RRTMG and CIESM following Eq. (10)-(12).

$$\widetilde{K}_{ext} = \frac{\int_{\lambda_{min}}^{\lambda_{max}} \beta_{ext}(\lambda)E(\lambda)d\lambda}{\int_{\lambda_{min}}^{\lambda_{max}} E(\lambda)d\lambda} \quad (10)$$

$$\widetilde{\varpi} = \frac{\int_{\lambda_{min}}^{\lambda_{max}} \varpi(\lambda)E(\lambda)d\lambda}{\int_{\lambda_{min}}^{\lambda_{max}} E(\lambda)d\lambda} \quad (11)$$

$$\tilde{g} \equiv \frac{\int_{\lambda_{min}}^{\lambda_{max}} g(\lambda)E(\lambda)d\lambda}{\int_{\lambda_{min}}^{\lambda_{max}} E(\lambda)d\lambda} \quad (12)$$

where $\tilde{K}_{ext}$, $\tilde{\varpi}$ and $\tilde{g}$ are band-averaged mass-averaged extinction coefficients, single-scattering albedo and asymmetry factor for the Voronoi scheme, respectively. E is assigned by the solar constant provided by Chance and Kurucz (2010) for the shortwave spectrum, and is replaced with the Planck function B(T) for longwave spectrum, T is an assuming cloud temperature of 233K according to Liou (1992). The coefficients of the polynomial expressions of the ice cloud band-averaged optical properties as functions of D_e are determined in each band interval to develop Voronoi scheme for shortwave and longwave spectrum as shown in Eq. (13)-(15).

$$\tilde{K}_{ext} \equiv a_0 \pm a_1/D_e \pm a_2/D_e^2 \quad (13)$$

$$\tilde{\varpi} \equiv b_0 \pm b_1 D_e \pm b_2 D_e^2 \pm b_3 D_e^3 \quad (14)$$

$$\tilde{g} \equiv c_0 \pm c_1 D_e \pm c_2 D_e^2 \pm c_3 D_e^3 \quad (15)$$

where a, b, c are coefficients as functions of band intervals.

In terms of other four existing schemes, the band-averaged optical properties of Mitchell, Yi and Baum-yang05 schemes are developed as functions of D_e following Eq. (13-15). Coefficients of Mitchell scheme can be obtained from the CIESM. Values of coefficients for Yi and Baum-yang05 schemes are listed in appendix A (Tables A1, A2, A3, and A4) provided from Zhao et al. (2018). Coefficients of the Fu scheme (default scheme in RRTMG) are obtained from the existing ice cloud band-averaged optical properties from RRTMG. Formulation of Fu scheme is similar to the Mitchell and Baum-yang05 schemes except using the generalized effective diameter (Fu, 1996). The generalized effective diameter of the Fu scheme is unified into D_e for comparability.

~~To describe the PSDs and calculate particle concentration per unit volume, we utilize 14408 groups of microphysical data (mainly including slope (N_0), intercept (μ), and dispersion (λ) of PSDs) derived from aircraft measurements obtained in 11 field campaigns (Heymsfield et al., 2013) to determine ice particle number density (n (L)) in the form of the gamma distribution (see equation (2)), where L is the ice particle maximum dimensions defined by equation (1). Detailed descriptions can be found in (Heymsfield et al., 2013). Assume that the extinction and scattering cross section is known as $\sigma_{e,s}$, and the absorption cross section can be given by $\sigma_a = \sigma_e - \sigma_s$. The extinction, scattering and absorption coefficients~~

can be calculated by equation (3). The single-scattering albedo and co-albedo can be defined as the ratio of the scattering and absorption coefficients to the extinction coefficient in the form of equation (4), respectively. Let the phase function corresponding to a volume of ice particles be P. Thus, P (μ, φ; μ', φ') denotes the redirection of the incoming intensity defined by (μ', φ') to the outgoing intensity defined by (μ, φ). The optical depth can be defined by equation (5). In plane-parallel atmospheres, changes in the diffuse intensity penetrating from below the layer considering multiple scattering processes is given by equation (6).

$$n(L) = N_0 L^{\mu} e^{-\lambda L}, \quad (2)$$

$$\beta_{e,s,a} = \int_{L_{min}}^{L_{max}} \sigma_{e,s,a} n(L) dL, \quad (3)$$

$$\varpi = \frac{\beta_s}{\beta_e}, \quad \text{or } 1 - \varpi = \frac{\beta_a}{\beta_e} \quad (4)$$

$$\tau = \int_z^{\infty} \beta_e \, dz, \quad (5)$$

$$I(\tau;\mu;\phi) = \frac{\varpi}{4\pi} \int_0^{2\pi} \int_{-1}^{1} I(\tau;\mu';\phi') P(\mu,\phi;\mu';\phi') d\mu' d\phi' + \frac{\varpi}{4\pi} F_{\theta} P(\mu,\phi;-\mu_0;\phi_0) e^{-\tau/\mu_0} + (1-\varpi) B[T(\tau)], \quad (6)$$

where I indicate the total (direct plus diffuse) radiance, B indicates Planck's function associated with thermal emissions, and Θ is the scattering angle. Obviously, extinction coefficients, single-scattering albedo and phase function, along with solar zenith angle are fundamental driving parameters within the transfer of diffuse intensity. Hence, to assess the effectiveness of the Voronoi ice particles model for application in the CAM5, it is necessary to develop polynomial expressions of the extinction coefficients, the single-scattering albedo and the asymmetry factor as functions of the effective diameter D_e.

$$D_e = \frac{3}{2} \frac{\int_{\lambda_{min}}^{\lambda_{max}} \int_{L_{min}}^{L_{max}} V(L) n(L) dL}{\int_{\lambda_{min}}^{\lambda_{max}} \int_{L_{max}}^{L_{max}} A(L) n(L) dL}, \quad (7)$$

$$K_{ext}(\lambda) = \frac{\int_{L_{min}}^{L_{max}} Q_{ext}(\lambda,L)A(L)n(L)dL}{\rho_{ice}\int_{L_{min}}^{L_{max}} V(L)n(L)dL}, \quad (8)$$

$$\varpi(\lambda) = \frac{\int_{L_{min}}^{L_{max}} Q_{sca}(\lambda,L)A(L)n(L)dL}{\int_{L_{min}}^{L_{max}} Q_{ext}(\lambda,L)A(L)n(L)dL}, \quad (9)$$

$$g(\lambda) = \frac{\int_{L_{min}}^{L_{max}} g(\lambda,L)\sigma_{sca}(\lambda,L)n(L)dL}{\int_{L_{min}}^{L_{max}} \sigma_{sca}(L)n(L)dL}, \quad (10)$$

$$\widetilde{K}_{ext} = \frac{\int_{\lambda_{min}}^{\lambda_{max}} \beta_{ext}(\lambda)S(\lambda)d\lambda}{\int_{\lambda_{min}}^{\lambda_{max}} S(\lambda)d\lambda}, \quad (11)$$

$$\widetilde{\varpi} = \frac{\int_{\lambda_{min}}^{\lambda_{max}} \varpi(\lambda)S(\lambda)d\lambda}{\int_{\lambda_{min}}^{\lambda_{max}} S(\lambda)d\lambda}, \quad (12)$$

$$\widetilde{g} = \frac{\int_{\lambda_{min}}^{\lambda_{max}} g(\lambda)S(\lambda)d\lambda}{\int_{\lambda_{min}}^{\lambda_{max}} S(\lambda)d\lambda}, \quad (13)$$

3.2 RRTMG and CIESM simulation experiments

~~### 3.2 The RRTMG and CAM5 simulations~~

The version of the RRTMG used in this study is the current version of the radiative transfer code applied in the CIESM (Mlawer et al., 1997; Iacono et al., 2008; Clough et al., 2005; available from http://rtweb.aer.com). RRTMG utilizes the correlated-k approach to calculate shortwave fluxes and heating rates efficiently and accurately for application to climate models. The version of RRTMG utilizes a two-stream method for radiative transfer calculation. RRTMG has 14 bands for shortwave spectrum and 16 longwave bands (see Table 1). Since the wavelength range is from 0.2 to 15 μm for the single-scattering property database of the Voronoi ICS model, ice cloud bulk optical properties of the default scheme (the Mitchell scheme) remain unchanged when bands are larger than 15 μm. To quantify the radiative flux differences caused by five schemes under the same conditions, we design an assuming ice cloud cases in standard tropics atmospheric profile in the RRTMG. The RRTMG sets are as follows, ice effective radius is set to 45 μm, the ice water path is set to 60 g m^{-2}, the ice

cloud top pressure/height is between 125.1 hPa and 245.5 hPa, and the cloud fraction is 50%, the solar zenith angles is set to 60 °. The vertical resolution is 60 levels for the standard tropics. The RRTMG is run by five ice cloud schemes under the same conditions, thus relative difference of fluxes can be explained by difference among five schemes. Five schemes are implemented in the CIESM to calculate the FSDS, FLDS, FSUTOA, FLUTOA and shortwave cloud forcing (SWCF) and longwave cloud forcing (LWCF). SWCF are defined as Eq. (16), LWCF is defined the same as SWCF but for longwave spectrum.

~~To clarify the radiative effects resulting from five different scheme, we utilize the RRTMG to calculate the upward and downward flux of five schemes for comparisons. RRTMG has 14 bands for SW spectrum and 16 longwave bands (see Table 1). RRTMG is the optional radiative transfer model applied in CAM5. Since the wavelength range is from 0.2 μm to 15 μm for Voronoi model database, ice cloud parameterization scheme remains unchanged in bands larger than 15 μm. To quantify the radiative flux differences caused by five schemes under the same conditions, we design an assuming ice cloud cases in standard tropics atmospheric profile in the RRTMG. Other detailed input parameters are shown in Table 2. The vertical resolution is 60 levels for the standard tropics. The RRTMG is run by five ice cloud schemes under the same conditions, thus relative difference of fluxes can be explained by difference among five schemes. Five schemes are implemented in the CAM5 for comparison of shortwave and longwave cloud forcing (SWCF and LWCF). SWCF are defined as equation (14), LWCF is defined the same with SWCF but for LW spectrum.~~

$$SWCF = F_{cloudy} - F_{clear} \quad (16)$$

~~$$SWCF = N(F_{cloudy} - F_{clear}), \quad (14)$$~~

where F_{cloudy} and F_{clear} are the difference between downward and upward fluxes for cloudy and clear conditions, respectively, and N is the cloud fraction. The ~~CAM5~~ CIESM is run in two ways: 1) the ~~CAM5~~ CIESM is run with the default Mitchell scheme for ice clouds and the default water cloud scheme to obtain SWCF and LWCF for the Mitchell scheme; 2) the ~~CAM5~~ CIESM is run by using the other four schemes (the Voronoi, Yi, Baum-yang05~~Baum-yang~~ and Fu scheme) in place of the Mitchell scheme, along with the default liquid water cloud scheme. Liquid water clouds adopt a spherical particle model, whose single-scattering properties are derived from the Lorenz-Mie theory (van de Hulst, 1957). Because the CIESM is unable to separate ice clouds from liquid clouds efficiently, the SWCF and LWCF for five schemes are under the

same liquid water cloud parameterization their differences are attributed to different ice habits and their scattering and absorption properties within five schemes. The CIESM run is integrated for 11 years in one-month increments, the initial first year is used for state initialization and stabilization, the last ten-year runs were utilized for analysis. Horizontal and vertical resolution of CIESM run experiment is set to 1.9° × 2.5° and 31 levels, respectively. The run is driven by prescribed climatological sea surface temperature and sea ice fraction with an annual cycle in the year 2000.~~The CAM run is integrated for 11 years in one-month increments, the initial first year is used for state initialization and stabilization, and the last ten-year runs were utilized for comparisons. Horizontal and vertical resolution of CAM5 run experiment is 1.9° × 2.5° and 31 levels. The run is driven by prescribed climatological sea surface temperature and sea ice fraction with an annual cycle in the year 2000. Within RRTMG and CAM5 simulations, water clouds adopt a spherical particle model, its single-scattering properties are derived from the Lorenz-Mie theory (Hulst, 1957). Since the CAM5 are unable to separate ice clouds from liquid clouds efficiently, the total SWCF/LWCF difference under the same water cloud parameterization is owing to the difference among five schemes.~~

4 Results and discussions

4.1 Band-averaged optical properties of the ice cloud

~~**4.1 Broadband bulk optical properties of the ice cloud**~~

Based on the integration over both PSDs and band intervals, band-averaged bulk optical properties of the Voronoi scheme are compared with Mitchell, Fu, Baum-yang05 and Yi schemes in Figure 4. The differences in ice cloud optical properties between the Voronoi and the other four existing schemes are shown in Figure 5. Since Fu scheme uses generalized effective diameter, the remaining four schemes use D_e. Horizontal axes in both Figure 4 and 5 are unified into D_e for comparability. Parameterized mass extinction coefficients, single-scattering albedo and asymmetry factor are plotted as functions of the D_e from 10 to 150 μm and 14 selected bands.

In Figure 4, mass extinction coefficients obtained from five schemes show uniformly negative correlation with D_e. Mass extinction coefficients exceed up to 0.2 m^2/g for D_e smaller than 20 μm and approach 0 for D_e larger than 100 μm. This could be partly related with the majority of small particles in PSDs for five schemes. Note that there is a minimum of mass

extinction coefficients between 3.08 and 3.85 μm. It could because that the real part of the refractive index reaches the minimum at 3 μm (Warren and Brandt, 2008; Yang et al., 2013a). This could weaken the scattering and extinction efficiency of ice particles. The single-scattering albedos obtained from five schemes approach 1.0 in visible bands (0.2-0.78 μm). In near-infrared bands (0.78-3.85 μm), the single-scattering albedos are inversely proportional to D_e. This result is related with the large real part in visible bands and small imaginary part of the complex refractive index of ice particles. The asymmetry factor obtained from five schemes increases with increasing wavelength for all D_e. From visible to near-infrared band, the asymmetry factor increases with the increasing D_e.

In Figure 5, differences in mass extinction coefficients between the Voronoi scheme and the other four schemes show the Voronoi scheme has slightly larger values than the Fu, Yi and Baum-yang05 schemes, but is smaller than the Mitchell scheme. For the single-scattering albedo, the Voronoi scheme has slightly larger single-scattering albedo than Fu and Mitchell schemes, and lower single-scattering albedo than Baum-yang05 and Yi schemes in infrared bands. This result may be because large ice particles are closer to geometric optics and have a greater proportion of absorption than small ice particles. The low asymmetry factor of the Voronoi scheme is because that the multifaceted shapes of the Voronoi ice model can result in significant side and backward scattering and reducing the forward scattered energy. Since the impacts of different size distribution assumptions on the bulk optical properties of ice cloud parameterization are negligible (Heymsfield et al., 2013, 2017), differences of band-averaged bulk optical properties between five schemes are originally rooted in different habits of ice particles and their single-scattering properties.~~Based on the integration of the single-scattering properties of the Voronoi ice model database over the PSDs and band intervals, the broadband bulk optical properties of the Voronoi scheme (Figure 3 a1-c1) are compared with properties obtained from the Mitchell (Figure 3 a2-c2), Fu (Figure 3 a3-c3), Baum-yang (Figure 3 a4-c4) and Yi (Figure 3 a5-c5) scheme for 14 bands from and D_e from 10 to 150 μm as shown in Figure 3 and their differences in Figure 4. For five schemes, it is found that the mass extinction coefficients show a negative correlation with D_e and are insensitive to wavelengths. The mass extinction coefficients exceed 0.2 m^2/g for D_e smaller than 20 μm, and is close to 0 m^2/g for D_e larger than 100 μm. The mass extinction coefficients of the Voronoi, Mitchell, Baum-yang and Yi scheme differ little as shown in Figure 4 A1, A3, A4, respectively, and the Fu scheme has lower mass extinction coefficients than the Voronoi scheme for D_e smaller than 20 μm, with the maximum negative~~

~~difference up to ~0.12m^2/g as shown in Figure 4 A2. As shown in Figure 3, there are low mass extinction coefficients in near-infrared bands (3.08−3.85 μm) due to the atmospheric window region which can lead to high transmittance. The single-scattering albedo obtained from five schemes (Figure 3 b1-b5) increases with decreasing wavelengths and is close to one in near-UV, visible and near-infrared band for all D_e. This result is related with the imaginary part of the refractive index of ice particles. Except for the Fu scheme, the single-scattering albedo obtained from the other four schemes decreases with the increases of D_e in near-infrared band. This result may be because large ice particles are closer to geometric optics and have a greater proportion of absorption than small ice particles that are closer to Rayleigh scattering. As shown in Figure 4 B1-B4, the single-scattering albedo of the Voronoi scheme is slightly larger than the Fu scheme and is smaller than the other three schemes in near-infrared bands. In Figure 3, the asymmetry factor obtained from five schemes (Figure 3 c1-c5) increases with increasing wavelength for all D_e. From visible to near-infrared band, the asymmetry factor increases with the growing D_e. With the increase of particle size, there are more absorption inside particles and decreasing single-scattering albedo, as well as decreasing side and backward scattering, resulting in more proportions of forward scattered energy. In Figure 4, the primary difference between the Voronoi scheme and the other four schemes lies in the asymmetry factor. Results show that the Voronoi scheme has the smallest asymmetry factor among five schemes, especially in visible and near-infrared band for D_e larger than 100 μm. This is because that the complex shapes of the Voronoi ice model with large particle size can result in significant side and backward scattering and reducing the forward scattered energy. It is consistent with findings of (Letu et al., 2016). For wavelength larger than 3 μm, the Mitchell scheme has the largest asymmetry factor compared with other four schemes, especially for D_e smaller than 50 μm. This highest asymmetry factor of the Mitchell scheme is also found compared among other schemes in the study of Zhao et al. (2018). It is in a good agreement with the results in Zhao et al., (2019). Overall, since the impacts of different size distribution assumptions on the bulk optical properties of ice cloud parameterization are negligible (Heymsfield et al., 2013; Heymsfield et al., 2017), differences of broadband bulk optical properties between five schemes are originally rooted in different habits of ice particles and their single-scattering properties.~~

4.2 RRTMG simulation results

After the parameterization, band-averaged optical properties of ice cloud from five schemes (Fu, Mitchell, Yi, Baum-yang05 and Voronoi) are subsequently parameterized as functions of D_e and 14 bands as shown in Figure 4.~~broadband bulk~~

~~single-scattering properties are subsequently parameterized as functions of D_e and 14 bands, broadband bulk optical properties of five schemes are compared to each other and their differences have been analyzed in section 4.1.~~ To illustrate and quantify the influence of optical properties of ice cloud on its radiative effects, an ideal experiment is designed to test the response of radiative flux to five ice cloud schemes under the same ~~assuming~~ idealized conditions. Band-averaged optical properties ~~Broadband bulk single-scattering properties of~~ for five schemes are subsequently implemented in RRTMG to simulate radiative fluxes under prescribed ice clouds in standard tropics profiles (Anderson et al., 1986) which have a high proportion of ice cloud coverage (Massie et al., 2002; Stubenrauch et al., 2013). According to observations of Hong and Liu (2015) ~~(Hong and Liu, 2015)~~, top and bottom pressure of ice cloud layer is set to 125.1 and 245.5 hPa, respectively, the D_e is set to 45 μm and ice water paths ~~(IWP)~~ equal to 60 g m^{-2}.

Shortwave radiative fluxes profiles of cloudy-sky for five schemes and clear-sky conditions are shown in Figure ~~5~~6. Obviously, the downward direct flux of five schemes should be the same due to the same cloud optical thickness. Figure 5 a1 show that cloudy-sky increases the upward flux due to larger cloud albedo compared with clear-sky conditions. Figure 5 a3 indicate cloudy-sky decrease downward flux due to the absorption effects inside the cloud. Net flux under cloudy-sky is smaller than clear-sky (Figure 5 a4), which can explain the cooling effects of ice cloud for SW spectrum. Figure 5 a3 show that cloudy-sky increase the downward diffuse fluxes owing to multiple and single scattering. Specific comparison of five schemes inside the black dotted region of Figure 5 a1 - a2, are enlarged and shown in Figure 5 a1' - a4'. In Figure 5 a1', upward fluxes of five schemes and their differences gradually increase from cloud bottom to cloud top, reaching to the maximum at the cloud top. The Voronoi and Mitchell scheme have higher upward fluxes (Figure 5 a1') and lower downward diffuse flux (Figure 5 a2') than the other three schemes. Differences of Voronoi scheme minus the Mitchell, Yi, Baum-yang and Fu scheme are 6-30 W/m^2 for TOA upward fluxes, and -10-(-40) W/m^2 for surface downward diffuse flux, -10- (-30) W/m2 for surface net fluxes, and -8-(-42) W/m^2 for TOA net fluxes. Radiative properties of Voronoi scheme in SW fluxes can be explained by its smaller asymmetry factor (Figure 3, 4) than the other four schemes, leading to smaller proportion of forward scattering and larger backward scattering. Thus, less SW flux reaching the ground and more upward flux for the Voronoi scheme compared with the other four schemes. Five schemes rank as the Voronoi, Mitchell, Yi, Baum-yang and Fu scheme for upward fluxes and the opposite rank for downward diffuse fluxes.

4.3 Climate model simulation results

~~## 4.3 CAM5 simulation results~~

As shown in RRTMG simulations in section 4.2, the influence of five ice cloud schemes (~~the~~ Voronoi, Yi, Mitchell, Baum-yang05~~Baum-yang~~ and Fu scheme~~s~~) on the radiative effects is evaluated under standard tropical atmospheric profiles, and with assumptions of idealized ice cloud microphysical properties as input data. Simulation results based upon radiative transfer model are capable of showing difference of ice cloud radiative effects for five schemes under some specific conditions, but are unable to demonstrate comprehensive performance of five schemes corresponding to real and complex atmospheric situation. To study the ice cloud modelling capabilities of five schemes in the climate model ~~as accurately as possible~~, the Voronoi, Yi, Baum-yang05~~Baum-yang~~ and Fu scheme~~s~~ are applied in the CIESM ~~CAM5 in place of the default scheme (Mitchell scheme)~~. Upwelling and downwelling fluxes and TOA SWCF and LWCF from CIESM simulations for five schemes compared with CERRES EBAF products are plotted in Figure 7 and 8, and their global-averaged values are listed in Table 3. The results show that the Voronoi scheme produced a lower difference of approximately -0.45 W/m^2 (1.1%) for the TOA shortwave cloud radiative forcing and -0.30 W/m^2 (1.4%) for the TOA longwave cloud radiative forcing compared with four existing schemes. For FSDS, the Voronoi scheme has the smallest downwelling fluxes at surface and is the closest to the EBAF products due to that the Voronoi scheme scatter the least energy in the forward direction. For FSUTOA, the Voronoi scheme possesses the largest upwelling fluxes compared to the other four schemes due to its strong backward scattering. For the longwave spectrum, the effects of the Voronoi scheme on the FLDS and FLUTOA is negligible.~~Figure 6 and Figure 7 show the 10-yr mean TOA SWCF and LWCF calculated from CERES SYN1deg products, and CAM5-simulated 10-yr average TOA SWCF and LWCF for five schemes. Obviously, SWCF and LWCF exhibit cooling and warming effects, respectively. It is found that SWCF and LWCF of SYN1deg products and CAM5 simulations are strong in tropics where frequent ice and liquid clouds occur. In CAM5 simulations for five schemes, the liquid water scheme remains unchanged, hence the difference of the total TOA SWCF and LWCF among five schemes are attributed to different ice habits and their scattering and absorption properties within five schemes. On a global average (Table 3), SWCF differences of CERES SYN1deg data minus CAM5 simulations in ascending order, are the Voronoi (-0.33 W/m^2), Mitchell (-1.11W/m^2), Yi (-2.03W/m^2), Baum-yang (-2.91 W/m^2) and Fu scheme (-4.02 W/m^2). LWCF differences of CERES~~

~~SYN1deg data minus CAM5 simulations in ascending order, are the Voronoi (-0.39 W/m^2), Mitchell (-0.76 W/m^2), Baum-yang (-0.86 W/m^2), Yi (-0.88 W/m^2) and Fu scheme (-1.11 W/m^2).~~

To discuss the influence of five schemes on the global distributions of SWCF and LWCF, the zonal ~~mean~~ average ~~analyses~~ analysis ~~are~~ is shown in Figure ~~8~~9. Results shows that the Voronoi scheme exhibits weaker cooling effects ~~and weaker warming effects~~ in tropical regions than the other four schemes~~, and reduce the differences of TOA SWCF and LWCF between the CAM5 simulations and CERES SYN1deg products.~~ As shown in RRTMG simulations (Figure 5), among five schemes, the Voronoi scheme has lowest SW net flux, which can obtain smallest SWCF according to equation (14). That is why the Voronoi scheme is closest to the CERES SYN1deg data over tropics region. Figure ~~9~~ 10 ~~show~~ displayed the distribution of differences between five schemes ~~minus~~ and CERES ~~SYN1deg mean values~~EBAF product. The differences box of Voronoi scheme are most concentrated on the zero line, and its statistical deviation is the smallest, which means the spatial distribution of cloud radiative effects of Voronoi scheme is closer to EBAF products~~CERES observed results~~ compared with other four existing schemes.

5 Conclusions

The optical property parameterization (Voronoi scheme) of the Voronoi ice crystal scattering (ICS) model is investigated for simulations of the ice cloud radiative properties in the Community Integrated Earth System Model (CIESM). The Voronoi scheme is completed based on the single-scattering properties of the Voronoi ICS database and particle size distributions from in-situ observations. The band-averaged optical properties of ice clouds including the mass extinction coefficients, single-scattering albedo and asymmetry factor of the Voronoi scheme are applied in the CIESM climate model and compared with those of the four existing schemes (Baum-yang05, Fu, Yi and Mitchell). The results show that the Voronoi scheme has a distinct feature of having the lowest asymmetry factor in the shortwave bands. This feature could be related to complex multifaceted shape of the Voronoi ICS model, and suggests that the Voronoi scheme can produce relatively stronger backward scattering compared with other schemes.

Radiative properties of ice clouds are firstly assessed in Rapid Radiative Transfer Model for General circulation model version (RRTMG) in the CIESM. The profiles of upward/downward fluxes from different ice cloud schemes are simulated

for the prescribed atmospheric condition. The RRTMG results show that the Voronoi scheme has the highest upward flux at the top of the atmosphere (TOA) and lowest downward flux at the surface when the solar zenith angle equals to 60 °. Therefore, the net flux of the Voronoi scheme is largest at the TOA and smallest at the surface compared with the other schemes, which are mostly due to its lowest asymmetry factor.

Five schemes (Baum-yang05, Fu, Yi, Mitchell and Voronoi) are then applied to the CIESM to simulate shortwave and longwave global total cloud radiative forcing at the TOA during 2001-2010. The accuracy of simulated 10-yr global total cloud radiative forcing from different schemes are evaluated by the Clouds and the Earth's Radiant Energy System (CERES) Energy Balanced And Filled (EBAF) product. The results show that the Voronoi scheme produced a lower difference for the TOA shortwave and longwave cloud radiative forcing compared with four existing schemes. Especially for the region (from 30°S to 30°N) where the ice clouds occur frequently, the Voronoi scheme provides the closest match with CERES EBAF product.

In conclusion, simulations of global averaged shortwave and longwave cloud radiative forcing at the TOA from five schemes are investigated through the EBAF product. We find that the Voronoi scheme present a better agreement with EBAF products than the other schemes, especially in the tropical region, which confirmed that the Voronoi ICS model has the possibility of ice cloud modelling capabilities in the climate model of the CIESM.~~This paper attempts to evaluate the influence of the irregularly shaped Voronoi model on the cloud radiative effects through parameterization (named Voronoi scheme) in the Community Atmosphere Model, Version 5 (CAM5). Bulk optical properties, standalone radiative model simulations based on RRTMG and CAM5 10-yr simulation results of Voronoi scheme are compared with the Mitchell scheme (the default scheme of the CAM5) and other four schemes (the Fu, Mitchell, Baum-yang and Yi). The conclusions are as follows.~~

~~Comparisons of broadband bulk ice cloud optical property indicate that the Voronoi scheme shows similar mass extinction coefficients and single-scattering albedos compared with the other four schemes. The Voronoi scheme produces a smaller asymmetry factor, which can cause stronger backward scattering, due to its complex shape. The RRTMG simulations exhibit the shortwave upward and downward flux profiles of five schemes. Results show that weaker absorption in the Voronoi scheme leads to more upward flux at the TOA but less downward flux at the surface in tropical cases, as well as reducing the~~

~~warming effects below the cloud more than the Mitchell scheme. Through 10-yr CAM5 simulations, this paper analysis the feedback effects of Voronoi scheme and existing four schemes on the climate system and their differences. The globally averaged TOA SWCF and LWCF induced by five ice cloud schemes produce 1.5% (6.3%), 2.2% (6.6%), 10.2% (6.4%), 9.3% (8.4%) and 6.8% (7.1%) difference against CERES, respectively.~~

~~In conclusion, Comparisons among Voronoi scheme, Baum-yang scheme, Yi scheme, Fu scheme, Mitchell scheme and CERES satellite observation show that Voronoi scheme generally agrees with satellite observations. The Voronoi model has the advantage of ice cloud modelling capabilities in CAM5 and possesses the potential for application in other global and zonal climate models. Tuning the ice cloud schemes in other climate models may effectively fix the discrepancy between the simulations and observations.~~

Data availability

The RRTMG code are available at http://rtweb.aer.com/rrtmg_sw_code.html, the CERES level3 EBAF products~~SYN1deg products~~ are available at https://ceres.larc.nasa.gov/data/.

Author contribution

Ming Li developed the ice cloud optical property parameterizations (Voronoi scheme) based on the single-scattering properties of Voronoi models, compared the band-averaged optical properties of the Voronoi scheme with the other four schemes (Mitchell, Yi, Baun-yang05 and Fu). Ming Li also compared the upward/downward flux profiles from five schemes through RRTMG standalone simulations and radiative properties of five schemes in CAM5 model simulations, as well as downloaded the CERES products and wrote the initial draft of this manuscript. Husi Letu designed the aims and structures of this study and assisted in developing the parameterization of ice cloud optical properties based on the Voronoi models. Husi Letu also provided the single-scattering property database of Voronoi models and helped in analyzing the single-scattering properties of Voronoi models, as well as guided the writings and revisions of the manuscript. Yiran Peng and Yanluan Lin assisted in developing the ice cloud optical property parameterization and provided the climate models, as well as guided the settings of climate model runs and reviewing the manuscript. Hiroshi Ishimoto developed the single-scattering property

database of Voronoi models, provided the database of Voronoi models and helped in the parameterization of ice cloud optical properties based on the single-scattering properties of Voronoi models. Takashi Y. Nakajima provided the single-scattering property database of Voronoi models, especially assisted in guiding the flowchart of this study and reviewed the manuscript. Anthony Baran guided the development of the ice cloud optical property parameterization and reviewed the paper. Zengyuan Guo assisted with the runs and design of the climate model simulations and helped with the review of the manuscript. Yonghui Lei assisted in analyzing the results and guided the flowchart of the study, as well as reviewed the manuscript. Jiancheng Shi assisted in designing the aims and structures of this study, guided the writings of the paper and helped reviewing the manuscript.

~~Husi Letu designed this research and helped guiding and reviewing the paper. Ming Li completed the experiments and wrote the initial draft of this manuscript. Yiran Peng, Yanluan Lin and ZengYuan Guo providing the climate model run platform and environment, as well as helped guiding the experiments and reviewing the paper. Anthony Baran helped reviewing and editing the paper. Yonghui Lei helped reviewing the paper.~~

Competing interests

The authors declare that they have no conflict of interests.

Acknowledgement

This work is supported by the Second Tibetan Plateau Scientific Expedition and Research Program (STEP) (Grant No. 2019QZKK0206), National Natural Science Foundation of China (Grant No. 42025504, 41771395) and International Partnership Programme of Bureau of International Cooperation Chinese Academy of Sciences (Contract No. 181811KYSB20190014).

References

Anderson, G. P., Clough, S. A., Kneizys, F. X., Chetwynd, J. H., and Shettle, E. P.: AFGL atmospheric constituent profiles (0.120km), 1986.

Baran, A. J.: A review of the light scattering properties of cirrus, J Quant Spectrosc Ra, 110, 1239-1260, 2009.

Baran, A. J.: From the single-scattering properties of ice crystals to climate prediction: A way forward, Atmos Res, 112, 45-69, 2012.

Baran, A. J. and Havemann, S.: Rapid computation of the optical properties of hexagonal columns using complex angular momentum theory, J Quant Spectrosc Ra, 63, 499-519, 1999.

Baran, A. J. and Labonnote, L. C.: A self-consistent scattering model for cirrus. I: The solar region, Q J Roy Meteor Soc, 133, 1899-1912, 10.1002/qj.164, 2007.

Baran, A. J., Hill, P., Furtado, K., Field, P., and Manners, J.: A Coupled Cloud Physics Radiation Parameterization of the Bulk Optical Properties of Cirrus and Its Impact on the Met Office Unified Model Global Atmosphere 5.0 Configuration, J Climate, 27, 7725-7752, 2014a.

Baran, A. J., Cotton, R., Furtado, K., Havemann, S., Labonnote, L. C., Marenco, F., Smith, A., and Thelen, J. C.: A self-consistent scattering model for cirrus. II: The high and low frequencies, Q J Roy Meteor Soc, 140, 1039-1057, 10.1002/qj.2193, 2014b.

Baum, B. A., Heymsfield, A. J., Yang, P., and Bedka, S. T.: Bulk scattering properties for the remote sensing of ice clouds. Part I: Microphysical data and models, Journal of Applied Meteorology, 44, 1885-1895, 2005a.

Baum, B. A., Yang, P., Heymsfield, A. J., Platnick, S., King, M. D., Hu, Y. X., and Bedka, S. T.: Bulk scattering properties for the remote sensing of ice clouds. Part II: Narrowband models, Journal of Applied Meteorology, 44, 1896-1911, 2005b.

Baum, B. A., Yang, P., Heymsfield, A. J., Schmitt, C. G., Xie, Y., Bansemer, A., Hu, Y. X., and Zhang, Z. B.: Improvements in Shortwave Bulk Scattering and Absorption Models for the Remote Sensing of Ice Clouds, J Appl Meteorol Clim, 50, 1037-1056, 2011.

Bi, L. and Yang, P.: Accurate simulation of the optical properties of atmospheric ice crystals with the invariant imbedding T-matrix method, J Quant Spectrosc Ra, 138, 17-35, 2014.

Bi, L., Yang, P., and Kattawar, G. W.: Edge-effect contribution to the extinction of light by dielectric disks and cylindrical particles, Appl Optics, 49, 4641-4646, 2010.

Bi, L., Yang, P., Kattawar, G., and Kahn, R.: Single-scattering properties of triaxial ellipsoidal particles for a size parameter range from the Rayleigh to geometric-optics regimes, Appl Optics, 48, 114-126, 2009.

Bi, L., Yang, P., Kattawar, G. W., and Mishchenko, M. I.: A numerical combination of extended boundary condition method and invariant imbedding method applied to light scattering by large spheroids and cylinders, J Quant Spectrosc Ra, 123, 17-22, 2013a.

Bi, L., Yang, P., Kattawar, G. W., and Mishchenko, M. I.: Efficient implementation of the invariant imbedding T-matrix method and the separation of variables method applied to large nonspherical inhomogeneous particles, J Quant Spectrosc Ra, 116, 169-183, 2013b.

Bi, L., Yang, P., Kattawar, G. W., Hu, Y. X., and Baum, B. A.: Scattering and absorption of light by ice particles: Solution by a new physical-geometric optics hybrid method, J Quant Spectrosc Ra, 112, 1492-1508, 2011.

C.-Labonnote, L., G., Brogniez, J.-C., Buriez, M., Doutriaux-Boucher, J.-F. Gayet, and A. Macke: Polarized light scattering by inhomogeneous hexagonal monocrystals: Validation with ADEOS-POLDER measurements, J Geophys Res-Atmos, 106, 12139-12153, 2001.

C.-Labonnote, L., Brogniez, G., Doutriaux-Boucher, M., Buriez, J.-C., Gayet, J.-F., and Chepfer, H.: Modeling of light scattering in cirrus clouds with inhomogeneous hexagonal monocrystals. Comparison with in-situ and ADEOS-POLDER measurements, Geophysical Research Letters - GEOPHYS RES LETT, 27, 113-116, 2000.

Cai, Q. and Liou, K. N.: Polarized-Light Scattering by Hexagonal Ice Crystals - Theory, Appl Optics, 21, 3569-3580, 1982.

Chance, K. and Kurucz, R. L.: An improved high-resolution solar reference spectrum for earth's atmosphere measurements in the ultraviolet, visible, and near infrared, J Quant Spectrosc Ra, 111, 1289-1295, 2010.

Chen, G., Yang, P., and Kattawar, G. W.: Application of the pseudospectral time-domain method to the scattering of light by nonspherical particles, Journal of the Optical Society of America a-Optics Image Science and Vision, 25, 785-790, 2008.

Clough, S. A., Shephard, M. W., Mlawer, E., Delamere, J. S., Iacono, M., Cady-Pereira, K., Boukabara, S., and Brown, P. D.: Atmospheric radiative transfer modeling: a summary of the AER codes, J Quant Spectrosc Ra, 91, 233-244, 2005.

Deschamps, P. Y., Breon, F. M., Leroy, M., Podaire, A., Bricaud, A., Buriez, J. C., and Seze, G.: The Polder Mission - Instrument Characteristics and Scientific Objectives, Ieee T Geosci Remote, 32, 598-615, 1994.

Doelling, D. R., Sun, M., Nguyen, L. T., Nordeen, M. L., Haney, C. O., Keyes, D. F., and Mlynczak, P. E.: Advances in Geostationary-Derived Longwave Fluxes for the CERES Synoptic (SYN1deg) Product, J Atmos Ocean Tech, 33, 503-521, 2016.

Doutriaux-Boucher, M., Buriez, J.-C., Brogniez, G., C.-Labonnote, L., and Baran, A.: Sensitivity of retrieved POLDER directional cloud optical thickness to various ice particle models, Geophysical Research Letters - GEOPHYS RES LETT, 27, 109-112, 2000.

Draine, B. T. and Flatau, P. J.: Discrete-Dipole Approximation for Scattering Calculations, Journal of the Optical Society of America a-Optics Image Science and Vision, 11, 1491-1499, 1994.

Fu, Q.: A new parameterization of an asymmetry factor of cirrus clouds for climate models, J Atmos Sci, 64, 4140-4150, 2007.

Fu, Q., Yang, P., and Sun, W. B.: An accurate parameterization of the infrared radiative properties of cirrus clouds for climate models, J Climate, 11, 2223-2237, Doi 10.1175/1520-0442(1998)011<2223:Aapoti>2.0.Co;2, 1998.

Fu, Q. A.: An accurate parameterization of the solar radiative properties of cirrus clouds for climate models, J Climate, 9, 2058-2082, 1996.

Groth, S. P., Baran, A. J., Betcke, T., Havemann, S., and Smigaj, W.: The boundary element method for light scattering by ice crystals and its implementation in BEM plus, J Quant Spectrosc Ra, 167, 40-52, 2015.

Havemann, S. and Baran, A. J.: Extension of T-matrix to scattering of electromagnetic plane waves by non-axisymmetric dielectric particles: application to hexagonal ice cylinders, J Quant Spectrosc Ra, 70, 139-158, 2001.

Heymsfield, A. J. and Miloshevich, L. M.: Parameterizations for the cross-sectional area and extinction of cirrus and stratiform ice cloud particles, J Atmos Sci, 60, 936-956, 2003.

Heymsfield, A. J., Schmitt, C., and Bansemer, A.: Ice Cloud Particle Size Distributions and Pressure-Dependent Terminal Velocities from In Situ Observations at Temperatures from 0 degrees to-86 degrees C, J Atmos Sci, 70, 4123-4154, 2013.

Heymsfield, A. J., Bansemer, A., Field, P. R., Durden, S. L., Stith, J. L., Dye, J. E., Hall, W., and Grainger, C. A.: Observations and parameterizations of particle size distributions in deep tropical cirrus and stratiform precipitating clouds: Results from in situ observations in TRMM field campaigns, J Atmos Sci, 59, 3457-3491, 2002.

Heymsfield, A. J., Krämer, M., Luebke, A., Brown, P., Cziczo, D. J., Franklin, C., Lawson, P., Lohmann, U., McFarquhar, G., Ulanowski, Z., and Van Tricht, K.: Cirrus Clouds, Meteorological Monographs, 58, 2.1-2.26, 2017.

Hong, Y. L. and Liu, G. S.: The Characteristics of Ice Cloud Properties Derived from CloudSat and CALIPSO Measurements, J Climate, 28, 3880-3901, 2015.

Hulst, H. C. v. d.: Light scattering by small particles, Structure of matter series, Wiley, New York,, xiii, 470 p. pp.1957.

Hurrell, J. W., Holland, M. M., Gent, P. R., Ghan, S., Kay, J. E., Kushner, P. J., Lamarque, J. F., Large, W. G., Lawrence, D., Lindsay, K., Lipscomb, W. H., Long, M. C., Mahowald, N., Marsh, D. R., Neale, R. B., Rasch, P., Vavrus, S., Vertenstein, M., Bader, D., Collins, W. D., Hack, J. J., Kiehl, J., and Marshall, S.: The Community Earth System Model A Framework for Collaborative Research, B Am Meteorol Soc, 94, 1339-1360, 2013.

Illingworth, A. J., Barker, H. W., Beljaars, A., Ceccaldi, M., Chepfer, H., Clerbaux, N., Cole, J., Delanoe, J., Domenech, C., Donovan, D. P., Fukuda, S., Hirakata, M., Hogan, R. J., Huenerbein, A., Kollias, P., Kubota, T., Nakajima, T., Nakajima, T. Y., Nishizawa, T., Ohno,

Y., Okamoto, H., Oki, R., Sato, K., Satoh, M., Shephard, M. W., Velazquez-Blazquez, A., Wandinger, U., Wehr, T., and van Zadelhoff, G.-J.: THE EARTHCARE SATELLITE The Next Step Forward in Global Measurements of Clouds, Aerosols, Precipitation, and Radiation, B Am Meteorol Soc, 96, 1311-1332, 2015.

Ishimoto, H., Masuda, K., Mano, Y., Orikasa, N., and Uchiyama, A.: Irregularly shaped ice aggregates in optical modeling of convectively generated ice clouds, J Quant Spectrosc Ra, 113, 632-643, 2012.

Labonnote, L. C., Brogniez, G., Buriez, J. C., Doutriaux-Boucher, M., Gayet, J. F., and Macke, A.: Polarized light scattering by inhomogeneous hexagonal monocrystals: Validation with ADEOS-POLDER measurements, J Geophys Res-Atmos, 106, 12139-12153, 2001.

Lawson, R. P., Baker, B., Pilson, B., and Mo, Q. X.: In situ observations of the microphysical properties of wave, cirrus, and anvil clouds. Part II: Cirrus clouds, J Atmos Sci, 63, 3186-3203, 2006.

Lawson, R. P., Woods, S., Jensen, E., Erfani, E., Gurganus, C., Gallagher, M., Connolly, P., Whiteway, J., Baran, A. J., May, P., Heymsfield, A., Schmitt, C. G., McFarquhar, G., Um, J., Protat, A., Bailey, M., Lance, S., Muehlbauer, A., Stith, J., Korolev, A., Toon, O. B., and Kramer, M.: A Review of Ice Particle Shapes in Cirrus formed In Situ and in Anvils, J Geophys Res-Atmos, 124, 10049-10090, 2019.

Letu, H., Nakajima, T. Y., and Matsui, T. N.: Development of an ice crystal scattering database for the global change observation mission/second generation global imager satellite mission: investigating the refractive index grid system and potential retrieval error, Appl Optics, 51, 6172-6178, 2012.

Letu, H., Ishimoto, H., Riedi, J., Nakajima, T. Y., Labonnote, L. C., Baran, A. J., Nagao, T. M., and Sekiguchi, M.: Investigation of ice particle habits to be used for ice cloud remote sensing for the GCOM-C satellite mission, Atmos Chem Phys, 16, 12287-12303, 2016.

Letu, H. S., Nagao, T. M., Nakajima, T. Y., Riedi, J., Ishimoto, H., Baran, A. J., Shang, H. Z., Sekiguchi, M., and Kikuchi, M.: Ice Cloud Properties From Himawari-8/AHI Next-Generation Geostationary Satellite: Capability of the AHI to Monitor the DC Cloud Generation Process, Ieee T Geosci Remote, 57, 3229-3239, 2018.

Letu, H. S., Yang, K., Nakajima, T. Y., Ishimoto, H., Nagao, T. M., Riedi, J., Baran, A. J., Ma, R., Wang, T. X., Shang, H. Z., Khatri, P., Chen, L. F., Shi, C. X., and Shi, J. C.: High-resolution retrieval of cloud microphysical properties and surface solar radiation using Himawari-8/AHI next-generation geostationary satellite, Remote Sensing of Environment, 239, 2020.

Lin, Y., Huang, X., Liang, Y., Qin, Y., Xu, S., & Huang, W., and al., e.: Community Integrated Earth SystemModel (CIESM): Description andevaluation., Journal of Advances in Modeling Earth Systems, 12, 0, 2020.

Lin Y L, H. X. M., Liang Y S, et al.: The Community Integrated Earth System Model (CIESM) from Tsinghua University and its plan for CMIP6 experiments, Climate Change Research, 15 (5), 0, 2020.

Liou, K.-N.: Radiation and cloud processes in the atmosphere: theory, observation and modeling, Oxford monographs on geology and geophysics, 20, Oxford University Press, New York, ix, 487 p. pp.1992.

Liou, K. N.: Influence of Cirrus Clouds on Weather and Climate Processes - a Global Perspective, Mon Weather Rev, 114, 1167-1199, 1986.

Liu, Q. H.: The PSTD algorithm: A time-domain method requiring only two cells per wavelength, Microwave and Optical Technology Letters, 15, 158-165, 1997.

Liu, Y. Z., Hua, S., Jia, R., and Huang, J. P.: Effect of Aerosols on the Ice Cloud Properties Over the Tibetan Plateau, J Geophys Res-Atmos, 124, 9594-9608, 2019.

Macke, A., Mueller, J., and Raschke, E.: Single scattering properties of atmospheric ice crystals, J Atmos Sci, 53, 2813-2825, Doi 10.1175/1520-0469(1996)053<2813:Sspoai>2.0.Co;2, 1996.

Macke, A., Mishchenko, M. I., Muinonen, K., and Carlson, B. E.: Scattering of Light by Large Nonspherical Particles - Approximation Versus T-Matrix Method, Optics Letters, 20, 1934-1936, 1995.

Massie, S., Gettelman, A., Randel, W., and Baumgardner, D.: Distribution of tropical cirrus in relation to convection, J Geophys Res-Atmos, 107, 2002.

Mishchenko, M. I. and Travis, L.: Capabilities and Limitations of a Current FORTRAN Implementation of the T-matrix Method for Randomly Oriented, Rotationally Symmetric Scatterers, Journal of Quantitative Spectroscopy and Radiative Transfer, 60, 309-324, 1998.

Mishchenko, M. I., Travis, L. D., and Mackowski, D. W.: T-matrix computations of light scattering by nonspherical particles: A review, J Quant Spectrosc Ra, 55, 535-575, 1996.

Mitchell, David, L., Liu, Yangang, Macke, and Andreas: Modeling Cirrus Clouds. Part II: Treatment of Radiative Properties, J. Atmos. Sci, 53, 2967-2988, 1996b.

Mitchell, D. L. and Arnott, W. P.: A Model Predicting the Evolution of Ice Particle-Size Spectra and Radiative Properties of Cirrus Clouds .2. Dependence of Absorption and Extinction on Ice Crystal Morphology, J Atmos Sci, 51, 817-832, 1994.

Mitchell, D. L., Baran, A. J., Arnott, W. P., and Schmitt, C.: Testing and comparing the modified anomalous diffraction approximation, J Atmos Sci, 63, 2948-2962, 2006.

Mitchell, D. L., Chai, S. K., Liu, Y. G., Heymsfield, A. J., and Dong, Y. Y.: Modeling Cirrus Clouds. Part I: Treatment of Bimodal Size Spectra and Case Study Analysis, J Atmos Sci, 53, 2952-2966, 1996a.

Morcrette, J. J., Barker, H. W., Cole, J. N. S., Iacono, M. J., and Pincus, R.: Impact of a New Radiation Package, McRad, in the ECMWF Integrated Forecasting System, Mon Weather Rev, 136, 4773-4798, 2008.

Nakajima, T., Nakajima, T., Yoshimori, K., Mishra, S., and Tripathi, S.: Development of a light scattering solver applicable to particles of arbitrary shape on the basis of the surface-integral equations method of Müller type. I. Methodology, accuracy of calculation, and electromagnetic current on the particle surface, Appl Optics, 48, 3526-3536, 2009.

Nakajima, T. Y., Ishida, H., Nagao, T. M., Hori, M., Letu, H., Higuchi, R., Tamaru, N., Imoto, N., and Yamazaki, A.: Theoretical basis of the algorithms and early phase results of the GCOM-C (Shikisai) SGLI cloud products, Progress in Earth and Planetary Science, 6, 2019.

Neale, R. B., Gettelman, A., Park, S., Conley, A. J., Kinnison, D., Marsh, D., Smith, A. K., Vitt, F., Morrison, H., and Cameronsmith, P.: Description of the NCAR Community Atmosphere Model (CAM 5.0), Tech. Note NCAR/TN-486+STR, Natl. Cent. for Atmos, Land Model .ncar Tech.note Ncar, tn-486+str, 2010.

Ramaswamy, V. and Ramanathan, V.: Solar Absorption by Cirrus Clouds and the Maintenance of the Tropical Upper Troposphere Thermal Structure, J Atmos Sci, 46, 2293-2310, 1989.

Rossow, W. B. and Schiffer, R. A.: Isccp Cloud Data Products, B Am Meteorol Soc, 72, 2-20, 1991.

Rossow, W. B. and Schiffer, R. A.: Advances in understanding clouds from ISCCP, B Am Meteorol Soc, 80, 2261-2287, 1999.

Stubenrauch, C. J., Rossow, W. B., Kinne, S., Ackerman, S., Cesana, G., Chepfer, H., Di Girolamo, L., Getzewich, B., Guignard, A., Heidinger, A., Maddux, B. C., Menzel, W. P., Minnis, P., Pearl, C., Platnick, S., Poulsen, C., Riedi, J., Sun-Mack, S., Walther, A., Winker, D., Zeng, S., and Zhao, G.: Assessment of Global Cloud Datasets from Satellites: Project and Database Initiated by the GEWEX Radiation Panel, B Am Meteorol Soc, 94, 1031-1049, 2013.

Sun, W. B., Fu, Q., and Chen, Z. Z.: Finite-difference time-domain solution of light scattering by dielectric particles with a perfectly matched layer absorbing boundary condition, Appl Optics, 38, 3141-3151, 1999.

Takano, Y. and Liou, K. N.: Solar Radiative-Transfer in Cirrus Clouds .1. Single-Scattering and Optical-Properties of Hexagonal Ice Crystals, J Atmos Sci, 46, 3-19, 1989.

van de Hulst, H. C.: Light scattering by small particles, Wiley, New York,, xiii, 470 p. pp.1957.

van Diedenhoven, B.: Remote Sensing of Crystal Shapes in Ice Clouds, in, 197-250, 10.1007/978-3-319-70808-9, 2018.

van Diedenhoven, B. and Cairns, B.: A Flexible Parameterization for Shortwave and Longwave Optical Properties of Ice Crystals and Derived Bulk Optical Properties for Climate Models, J Atmos Sci, 77, 1245-1260, 2020.

van Diedenhoven, B., Fridlind, A. M., Cairns, B., and Ackerman, A. S.: Variation of ice crystal size, shape, and asymmetry parameter in tops of tropical deep convective clouds, J Geophys Res-Atmos, 119, 11809-11825, 2014b.

Walters, D., Baran, A. J., Boutle, I., Brooks, M., Earnshaw, P., Edwards, J., Furtado, K., Hi, P., Lock, A., Manners, J., Morcrette, C., Mulcahy, J., Sanchez, C., Smith, C., Stratton, R., Tennant, W., Tomassini, L., Van Weverberg, K., Vosper, S., Willett, M., Browse, J., Bushell, A., Carslaw, K., Dalvi, M., Essery, R., Gedney, N., Hardiman, S., Johnson, B., Johnson, C., Jones, A., Jones, C., Mann, G., Milton, S., Rumbold, H., Sellar, A., Ujiie, M., Whitall, M., Williams, K., and Zerroukat, M.: The Met Office Unified Model Global Atmosphere 7.0/7.1 and JULES Global Land 7.0 configurations, Geoscientific Model Development, 12, 1909-1963, 2019.

Wang, P. H., Minnis, P., McCormick, M. P., Kent, G. S., and Skeens, K. M.: A 6-year climatology of cloud occurrence frequency from stratospheric aerosol and gas experiment II observations (1985-1990), J Geophys Res-Atmos, 101, 29407-29429, 1996.

Warren, S. G. and Brandt, R. E.: Optical constants of ice from the ultraviolet to the microwave: A revised compilation, J Geophys Res-Atmos, 113, 2008.

Wendling, P., Wendling, R., and Weickmann, H.: Scattering of solar radiation by hexagonal ice crystals, Appl Optics, 18, 2663-2671, 1979.

Yan, H. R. and Wang, T. H.: Ten Years of Aerosol Effects on Single-Layer Overcast Clouds over the US Southern Great Plains and the China Loess Plateau, Advances in Meteorology, 2020, 2020.

Yang, P. and Liou, K. N.: Light-Scattering by Hexagonal Ice Crystals - Comparison of Finite-Difference Time-Domain and Geometric Optics Models, Journal of the Optical Society of America a-Optics Image Science and Vision, 12, 162-176, 1995.

Yang, P. and Liou, K. N.: Geometric-optics-integral-equation method for light scattering by nonspherical ice crystals, Appl Optics, 35, 6568-6584, 1996a.

Yang, P. and Liou, K. N.: Finite-difference time domain method for light scattering by small ice crystals in three-dimensional space, Journal of the Optical Society of America a-Optics Image Science and Vision, 13, 2072-2085, 1996b.

Yang, P., Liou, K. N., Wyser, K., and Mitchell, D.: Parameterization of the scattering and absorption properties of individual ice crystals, J Geophys Res-Atmos, 105, 4699-4718, 2000a.

Yang, P., Hioki, S., Saito, M., Kuo, C. P., Baum, B. A., and Liou, K. N.: A Review of Ice Cloud Optical Property Models for Passive Satellite Remote Sensing, Atmosphere, 9, 2018.

Yang, P., Liou, K. N., Bi, L., Liu, C., Yi, B. Q., and Baum, B. A.: On the Radiative Properties of Ice Clouds: Light Scattering, Remote Sensing, and Radiation Parameterization, Advances in Atmospheric Sciences, 32, 32-63, 2015.

Yang, P., Bi, L., Baum, B. A., Liou, K. N., Kattawar, G. W., Mishchenko, M. I., and Cole, B.: Spectrally Consistent Scattering, Absorption, and Polarization Properties of Atmospheric Ice Crystals at Wavelengths from 0.2 to 100 μm, J Atmos Sci, 70, 330-347, 2013a.

Yang, P., Bi, L., Baum, B. A., Liou, K. N., Kattawar, G. W., Mishchenko, M. I., and Cole, B.: Spectrally Consistent Scattering, Absorption, and Polarization Properties of Atmospheric Ice Crystals at Wavelengths from 0.2 to 100 mu m, J Atmos Sci, 70, 330-347, 10.1175/Jas-D-12-039.1, 2013b.

Yang, P., Wei, H. L., Huang, H. L., Baum, B. A., Hu, Y. X., Kattawar, G. W., Mishchenko, M. I., and Fu, Q.: Scattering and absorption property database for nonspherical ice particles in the near- through far-infrared spectral region, Appl Optics, 44, 5512-5523, 2005.

Yee, K. S.: Numerical solution of initial boundary value problems involving maxwell's equations in isotropic media, IEEE Transactions on Antennas & Propagation, 14, 302-307, 1966.

Yi, B. Q., Rapp, A. D., Yang, P., Baum, B. A., and King, M. D.: A comparison of Aqua MODIS ice and liquid water cloud physical and optical properties between collection 6 and collection 5.1: Cloud radiative effects, J Geophys Res-Atmos, 122, 4550-4564, 2017.

Yi, B. Q., Yang, P., Baum, B. A., L'Ecuyer, T., Oreopoulos, L., Mlawer, E. J., Heymsfield, A. J., and Liou, K. N.: Influence of Ice Particle Surface Roughening on the Global Cloud Radiative Effect, J Atmos Sci, 70, 2794-2807, 2013.

Yurkin, M. and Hoekstra, A.: The discrete-dipole-approximation code ADDA: Capabilities and known limitations, Journal of Quantitative Spectroscopy and Radiative Transfer, 112, 2011a.

Yurkin, M. A. and Hoekstra, A. G.: The discrete dipole approximation: An overview and recent developments, J Quant Spectrosc Ra, 106, 558-589, 2007.

Yurkin, M. A. and Hoekstra, A. G.: The discrete-dipole-approximation code ADDA: Capabilities and known limitations, J Quant Spectrosc Ra, 112, 2234-2247, 2011b.

Yurkin, M. A., Maltsev, V. P., and Hoekstra, A. G.: The discrete dipole approximation for simulation of light scattering by particles much larger than the wavelength, J Quant Spectrosc Ra, 106, 546-557, 2007.

Zhang, H., Chen, Q., and Xie, B.: A new parameterization for ice cloud optical properties used in BCC-RAD and its radiative impact, J Quant Spectrosc Ra, 150, 76-86, 2015.

Zhang, M. H., Lin, W. Y., Klein, S. A., Bacmeister, J. T., Bony, S., Cederwall, R. T., Del Genio, A. D., Hack, J. J., Loeb, N. G., Lohmann, U., Minnis, P., Musat, I., Pincus, R., Stier, P., Suarez, M. J., Webb, M. J., Wu, J. B., Xie, S. C., Yao, M. S., and Zhang, J. H.: Comparing clouds and their seasonal variations in 10 atmospheric general circulation models with satellite measurements, J Geophys Res-Atmos, 110, Artn D15s0210.1029/2004jd005021, 2005.

Zhao, W. J., Peng, Y. R., Wang, B., Yi, B. Q., Lin, Y. L., and Li, J. N.: Comparison of three ice cloud optical schemes in climate simulations with community atmospheric model version 5, Atmos Res, 204, 37-53, 2018.

Table Caption:

Table 1. Nomenclature

Table 2. Shortwave and longwave bands set in the RRTMG

Table 3. TOA upwelling and downwelling surface fluxes (W m-2) and TOA SWCF and LWCF (W m-2) for five schemes compared with CERRES EBAF products. Numbers in parentheses are differences between five scheme simulations and CERES EBAF products.

880

Table 1. Nomenclature

L	Particle maximum diameter (μm)
λ	Wavelength (μm)
SZP	Size parameter (unitless)
$n(L)$	Particle concentration (cm^{-3})
N_0	Intercept coefficient of $n(L)$ (unitless)
λ^*	Slope coefficient of $n(L)$ (unitless)
μ	Dispersion coefficient of $n(L)$ (unitless)
PSD	Particle size distribution defined by N_0, λ^*, μ and L
TOA	Top of atmosphere
$\beta_{e,s,a}$	Extinction, scattering and absorption coefficients
$\sigma_{e,s,a}$	Extinction, scattering, absorption cross section
θ	Inclination to the upward normal direction scattering angle
μ, μ'	Cosines of θ, incoming and outgoing intensity direction, respectively
φ, φ'	Incoming and outgoing intensity azimuthal angle in reference to the x axis, respectively
P	Phase function regulated by μ, ϕ, μ', ϕ'
z	Upper limit of the outer boundary
τ	Optical thickness
I	Total (direct plus diffuse) radiance
$B[T]$	Planck's function
$J(\tau;\mu;\varphi)$	Source function
D_e	Effective particle diameter
$Q_{ext,sca,}(\lambda,L)$	Extinction efficiency and scattering efficiency

$V(L)$	Ice particle volume (μm^3)
$A(L)$	Average geometrical cross section (μm^2)
$K_{ext}(\lambda), \widetilde{K}_{ext}$	Spectral and band-averaged of mass extinction coefficients
$\varpi(\lambda), \widetilde{\varpi}$	Spectral and band-averaged single-scattering albedo
$g(\lambda), \tilde{g}$	Spectral and band-averaged asymmetry factor
N	Cloud fraction
F_{cloudy}	Net fluxes of cloudy conditions
F_{clear}	Net fluxes of clear conditions
FSDS	Downwelling shortwave flux at the surface
FLDS	Downwelling longwave flux at the surface
FSUTOA	Upwelling shortwave flux at the top of atmosphere
FLUTOA	Upwelling longwave flux at the top of atmosphere
SWCF	Shortwave cloud forcing
LWCF	Longwave cloud forcing

~~Tables:~~

Table 2. Shortwave and longwave bands in the RRTMG

Shortwave		Longwave	
Band	μm	Band	cm-1
16	3.08–3.85	1	10–350
17	2.5–3.08	2	350–500
18	2.15–2.5	3	500–630
19	1.94–2.15	4	630–700
20	1.63–1.94	5	700–820
21	1.3–1.63	6	820–980
22	1.24–1.3	7	980–1080
23	0.78–1.24	8	1080–1180
24	0.63–0.78	9	1180–1390
25	0.44–0.63	10	1390–1480
26	0.34–0.44	11	1480–1800
27	0.26–0.34	12	1800–2080
28	0.2–0.26	13	2080–2250
29	3.85–12.2	14	2250–2380
		15	2380–2600
		16	2600–3250

Table 2. Input parameter settings in RRTMG

Cases	Pressure (hPa)	Ice water path (g/m^2)	Ice particle effective size (μm)	Cloud fraction (%)	Solar zenith angle (°θ)	Surface albedo
High ice cloud	125.1 - 245.5	60	45	0.5	60	0.1

Table 3. TOA upwelling and downwelling surface fluxes (W m^{-2}) and TOA SWCF and LWCF (W m^{-2}) for five schemes compared with CERRES EBAF products. Numbers in parentheses are differences between five scheme simulations and CERES EBAF products.

	CERES EBAF	Mitchell scheme	Voronoi scheme	Yi scheme	Baum-yang05 scheme	Fu scheme
FSDS	161.54	163.3 (1.76)	162.13 (0.59)	164.11 (2.57)	164.48 (2.94)	164.26 (2.72)
FLDS	309.98	298.9 (-11.08)	298.37 (-11.61)	298.11 (-11.87)	298.62 (-11.36)	299.31 (-10.67)
FSUTOA	102.20	102.79 (0.59)	104.79 (2.59)	102.65 (0.45)	102.58 (0.38)	100.36 (-1.84)
FLUTOA	222.52	217.98 (-4.54)	218.3 (-4.22)	217.67 (-4.85)	218.38 (-4.14)	218.7 (-3.82)
SWCF	-42.52	-43.73 (-1.21)	-42.97 (-0.45)	-44.67 (-2.15)	-45.55 (-3.03)	-46.66 (-4.14)
LWCF	20.88	20.21 (-0.67)	20.58 (-0.30)	20.09 (-0.79)	20.11 (-0.77)	19.86 (-1.02)

940

945

950

Table3. TOA SWCF and LWCF for five schemes and satellite observations.

	Baum-yang scheme	Fu scheme	Yi scheme	Mitchell scheme	Voronoi scheme	CERES SYN1deg
SWCF	-45.55 (2.91)	-46.66 (4.02)	-44.67 (2.03)	-43.73 (1.09)	-42.97 (0.33)	-42.64
LWCF	20.11 (0.86)	19.86 (1.11)	20.09 (0.88)	20.21 (0.76)	20.58 (0.39)	20.97

-

Figure Captions:

Figure 1. Single-scattering properties (extinction efficiency, single-scattering albedo and asymmetry factor) of Voronoi model from the composite method based on the FDTD, GOIE, and GOM methods at the wavelengths of (a) 0.64 μm and (b) 2.21μm.

Figure 2. Variations of ice particle size distributions for different temperature.

Figure 3. Flowchart of the investigation of ice cloud modelling capabilities for the irregularly shaped Voronoi models in climate simulations

Figure 4. The comparison of (top row) mass extinction coefficients, (middle row) single-scattering albedo and (bottom row) asymmetry factor as functions of effective diameter and 14 shortwave bands for (a) Voronoi, (b) Mitchell, (c) Fu, (d) Baum-yang05, and (e) Yi schemes.

Figure 5. The (a) Mitchell, (b) Fu, (c) Baum-yang05 and (d) Yi schemes minus the Voronoi scheme differences (%) in (top row) mass extinction coefficients, (middle row) single-scattering albedo and (bottom row) asymmetry factor as functions of effective diameter and 14 shortwave bands.

Figure 6. Shortwave (a) upward fluxes, (b) diffuse downward fluxes, (c) downward total fluxes and (d) net fluxes for the Voronoi, Mitchell, Fu, Baum-yang05, Yi schemes and clear conditions (blue line) for standard tropical atmospheric profile. Graphics in black dotted box are magnified and displayed in (e)-(h).

Figure 7. The 10-yr global average CIESM-based TOA SWCF simulations for Voronoi, Mitchell, Fu, Baum-yang05 and Yi schemes and corresponding CERES EBAF products during 2001-2010.

Figure 8. Same as the Figure 7, but for TOA LWCF.

Figure 9. Comparison of 10-yr zonally averaged annual mean (a) SWCF and (b) LWCF between the Voronoi, Mitchell, Fu, Baum-yang05, Yi schemes and CERES EBAF. EBAF minus five schemes differences of (c) SWCF and (d) LWCF.

Figure 10. Box analysis of zonal distributions of 10-yr annual mean SWCF (left) and LWCF (right) difference between the Mitchell, Voronoi, Fu, Baum-yang05, Yi scheme and EBAF products, respectively.

995

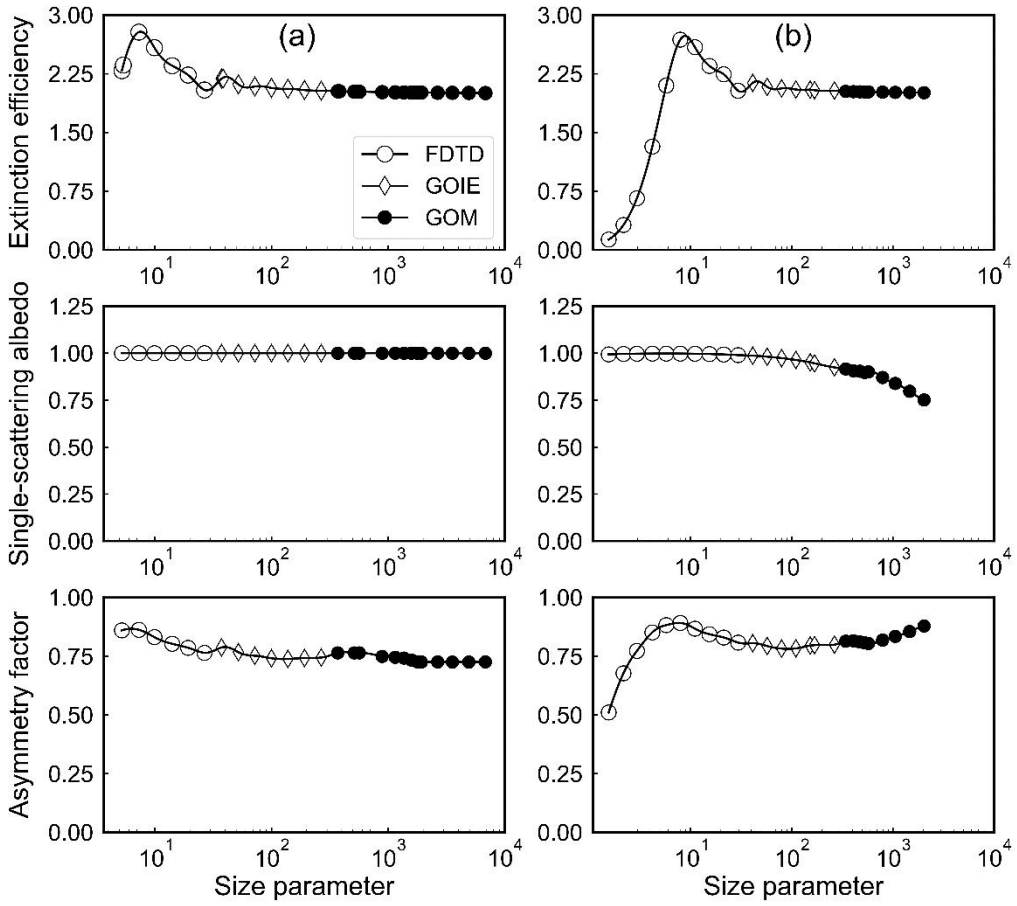

1000 Figure 1. Single-scattering properties (extinction efficiency, single-scattering albedo and asymmetry factor) of Voronoi model from the composite method based on the FDTD, GOIE, and GOM methods at the wavelengths of (a) 0.64 μm and (b) 2.21μm.

1005

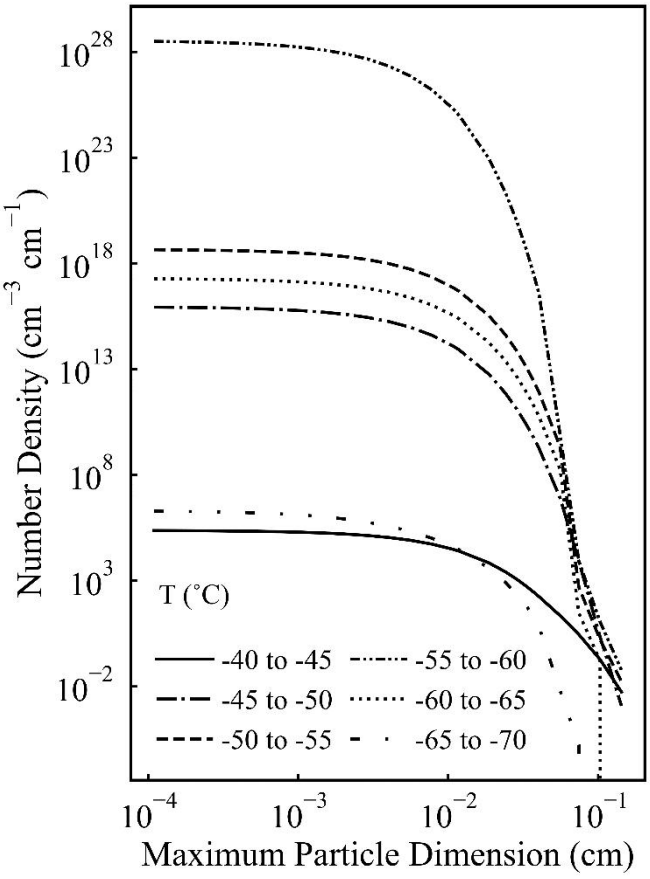

Figure 2. Variations of ice particle size distributions for different temperature.

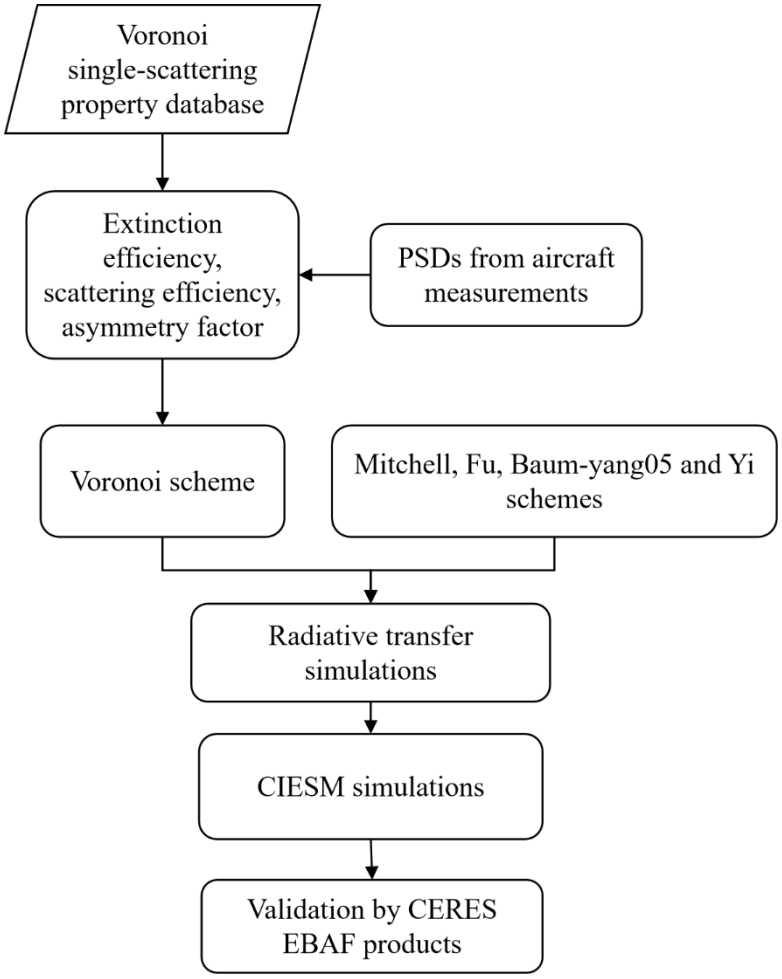

Figure 3. Flowchart of the investigation of ice cloud modelling capabilities for the irregularly shaped Voronoi models in climate simulations.

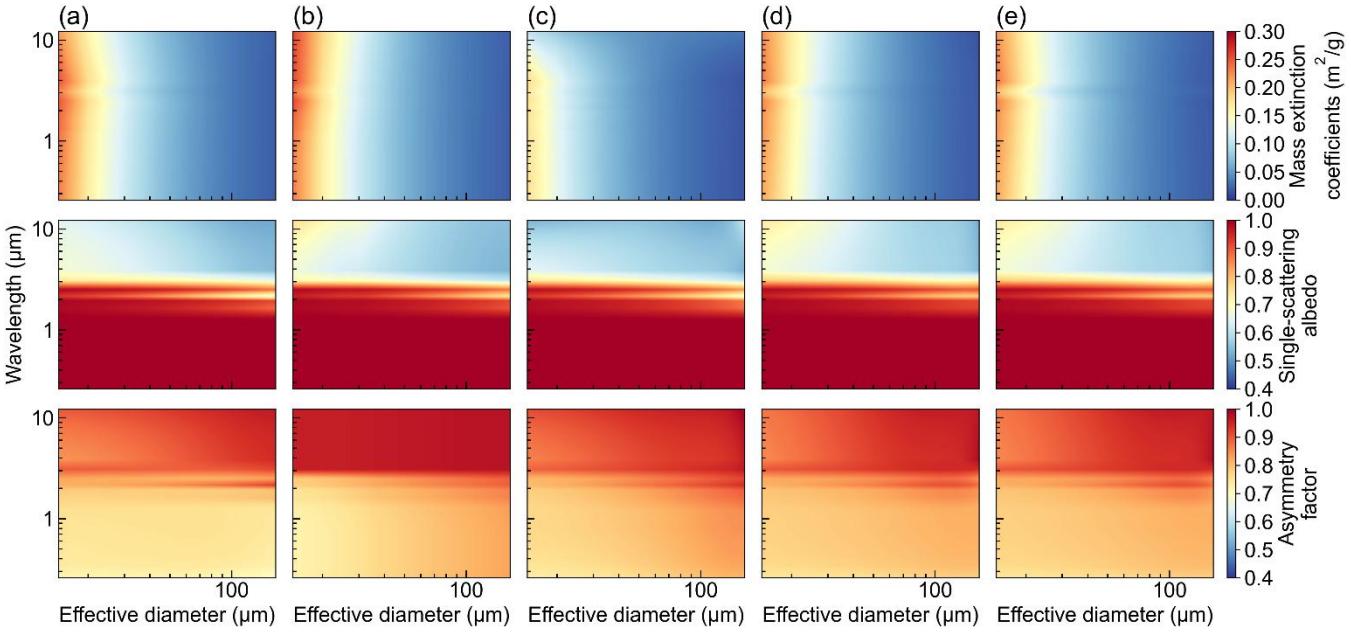

Figure 4. The comparison of (top row) mass extinction coefficients, (middle row) single-scattering albedo and (bottom row) asymmetry factor as functions of effective diameter and 14 shortwave bands for (a) Voronoi, (b) Mitchell, (c) Fu, (d) Baum-yang05, and (e) Yi schemes.

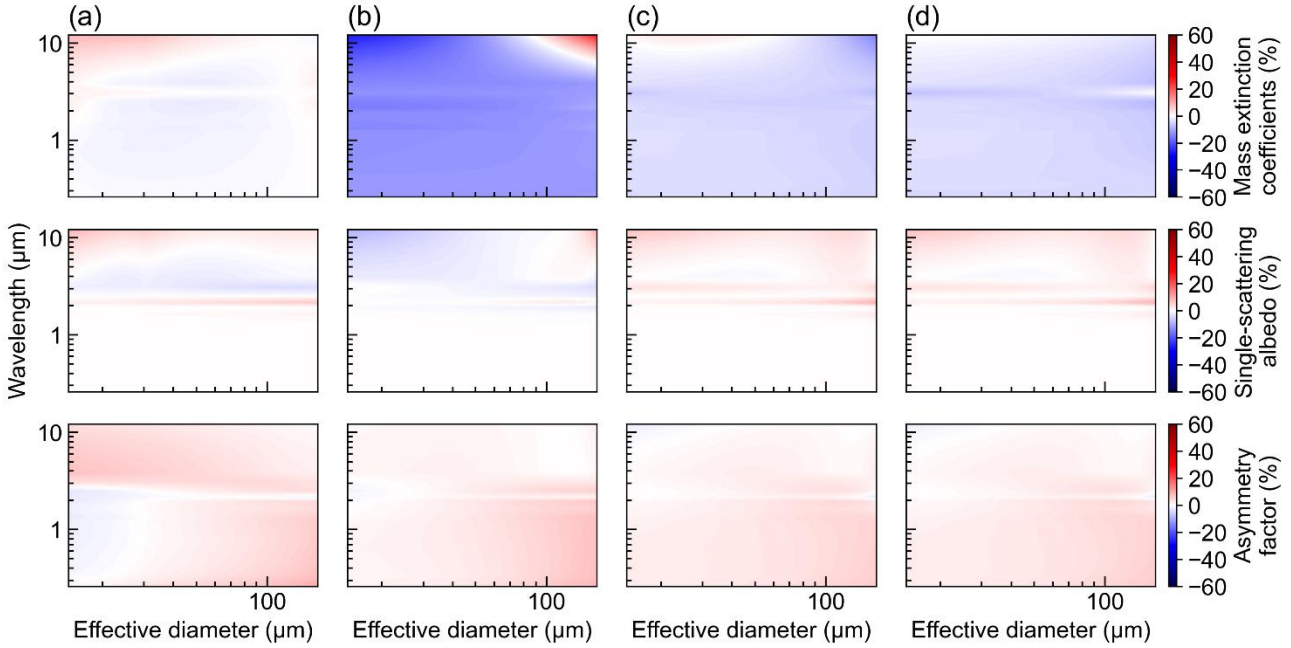

Figure 5. The (a) Mitchell, (b) Fu, (c) Baum-yang05 and (d) Yi schemes minus the Voronoi scheme differences (%) in (top row) mass extinction coefficients, (middle row) single-scattering albedo and (bottom row) asymmetry factor as functions of effective diameter and 14 shortwave bands.

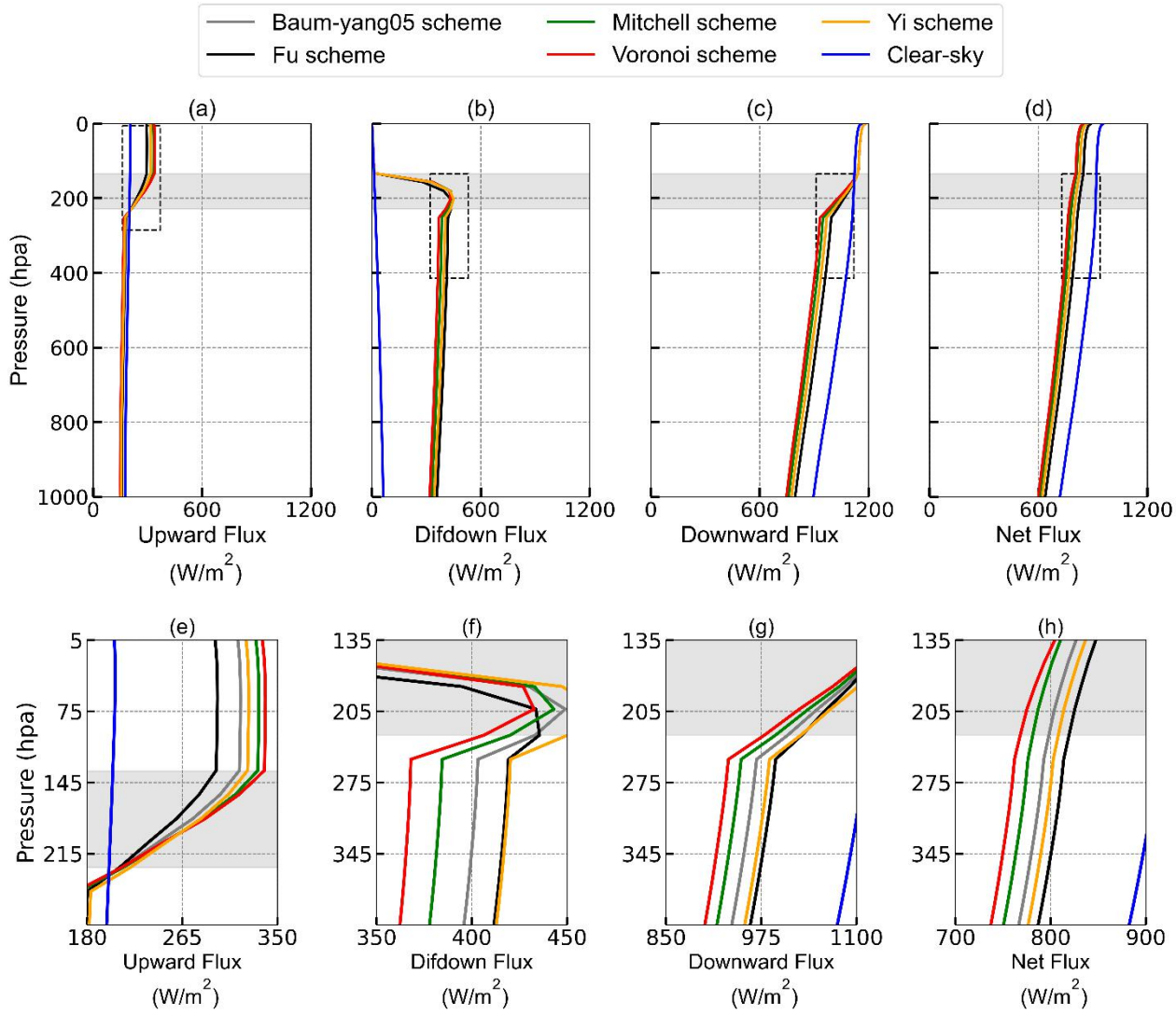

Figure 6. Shortwave (a) upward fluxes, (b) diffuse downward fluxes, (c) downward total fluxes and (d) net fluxes for the Voronoi, Mitchell, Fu, Baum-yang05, Yi schemes and clear conditions (blue line) for standard tropical atmospheric profile. Graphics in black dotted box are magnified and displayed in (e)-(h).

1050

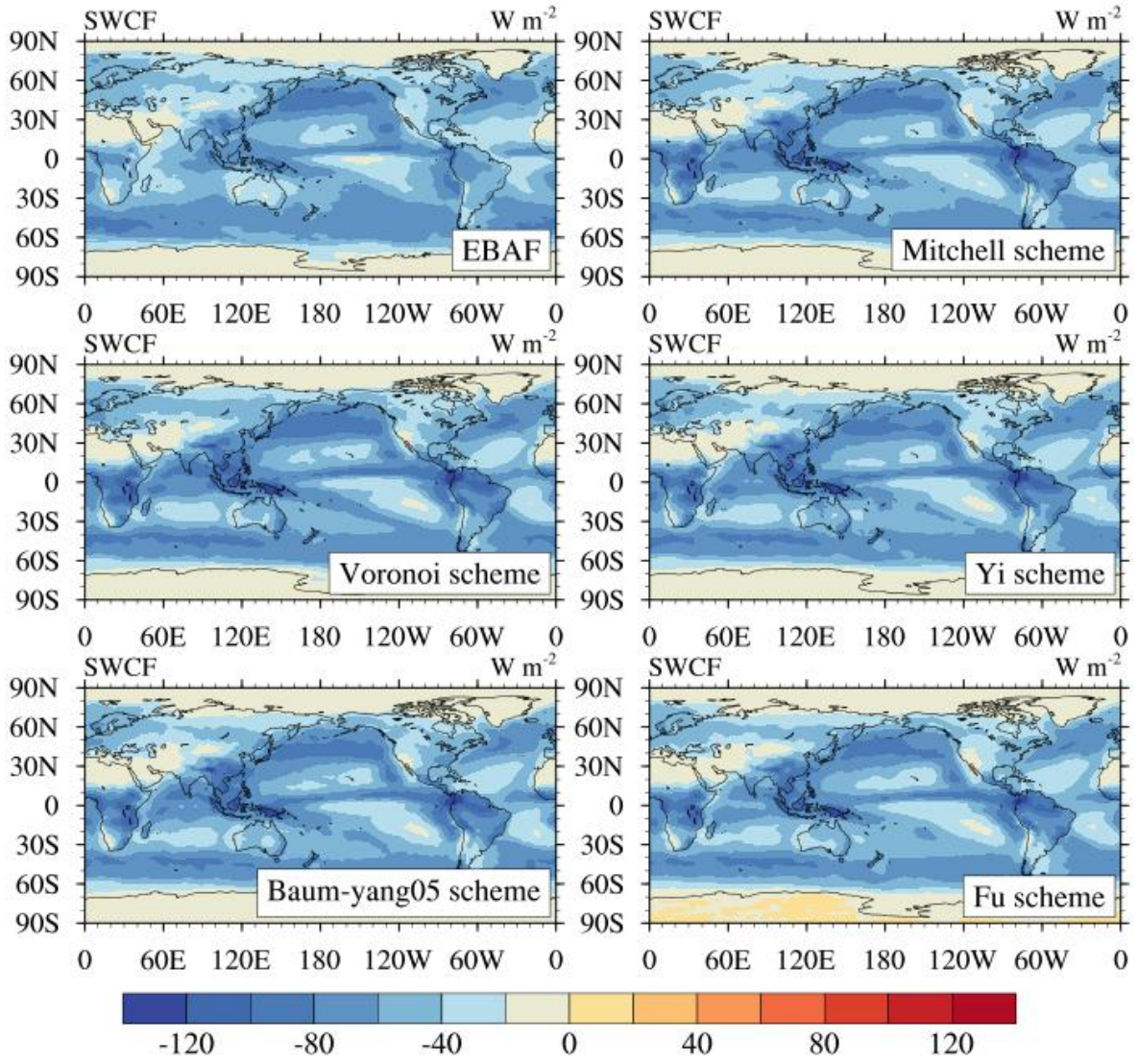

Figure 7. The 10-yr global average CIESM-based TOA SWCF simulations for Voronoi, Mitchell, Fu, Baum-yang05 and Yi schemes and corresponding CERES EBAF products during 2001-2010.

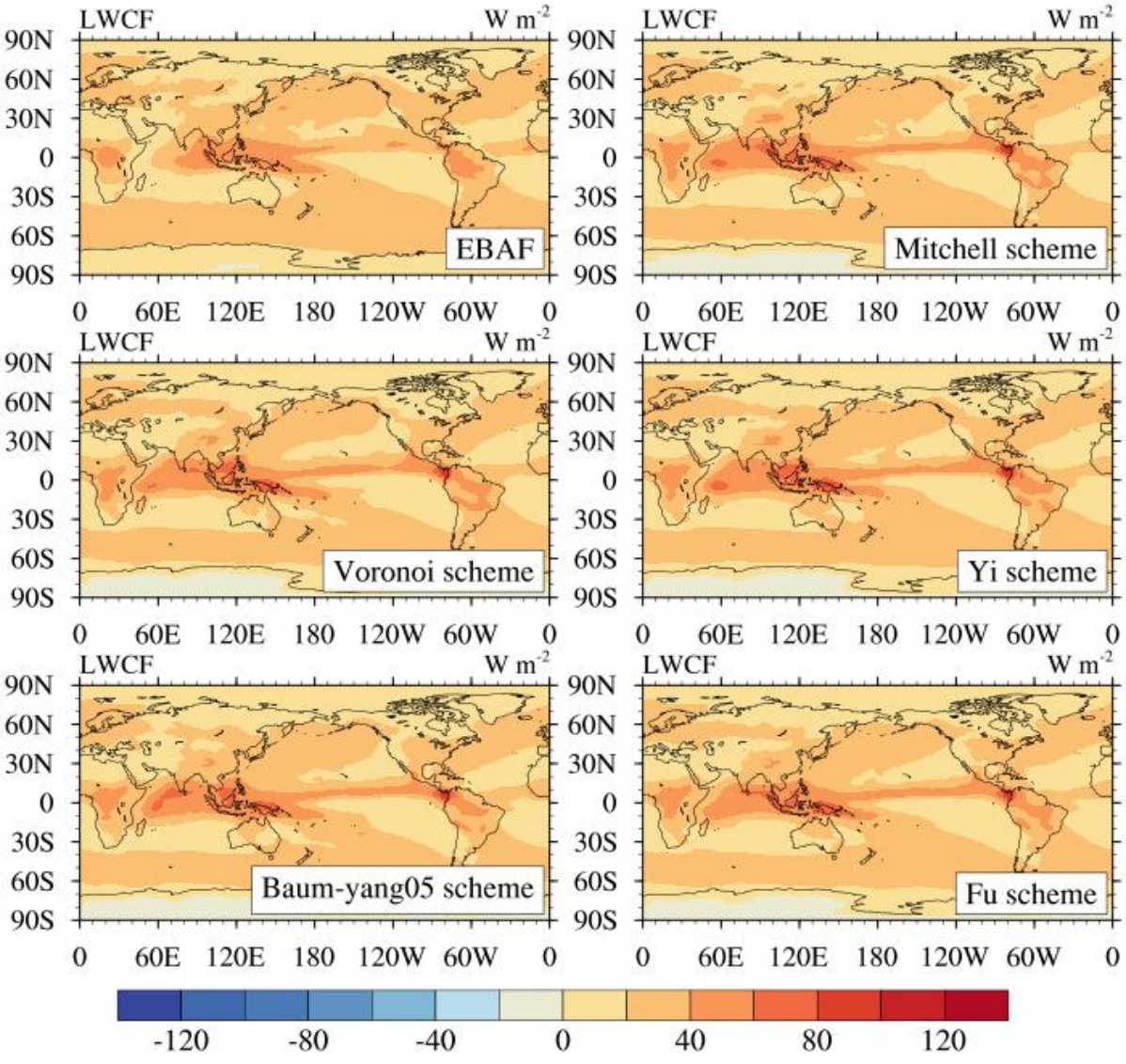

Figure 8. Same as the Figure 7, but for TOA LWCF.

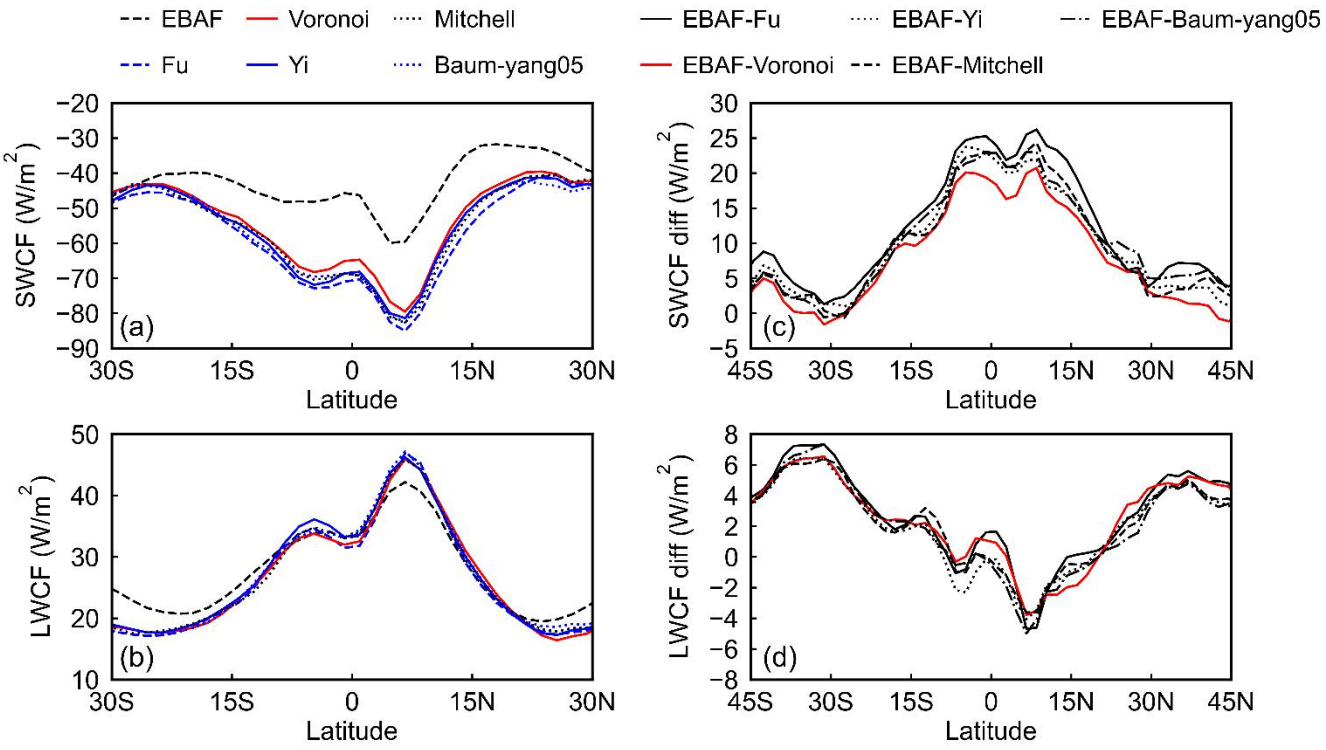

1065 Figure 9. Comparison of 10-yr zonally averaged annual mean (a) SWCF and (b) LWCF between the Voronoi, Mitchell, Fu, Baum-yang05, Yi schemes and CERES EBAF. EBAF minus five schemes differences of (c) SWCF and (d) LWCF.

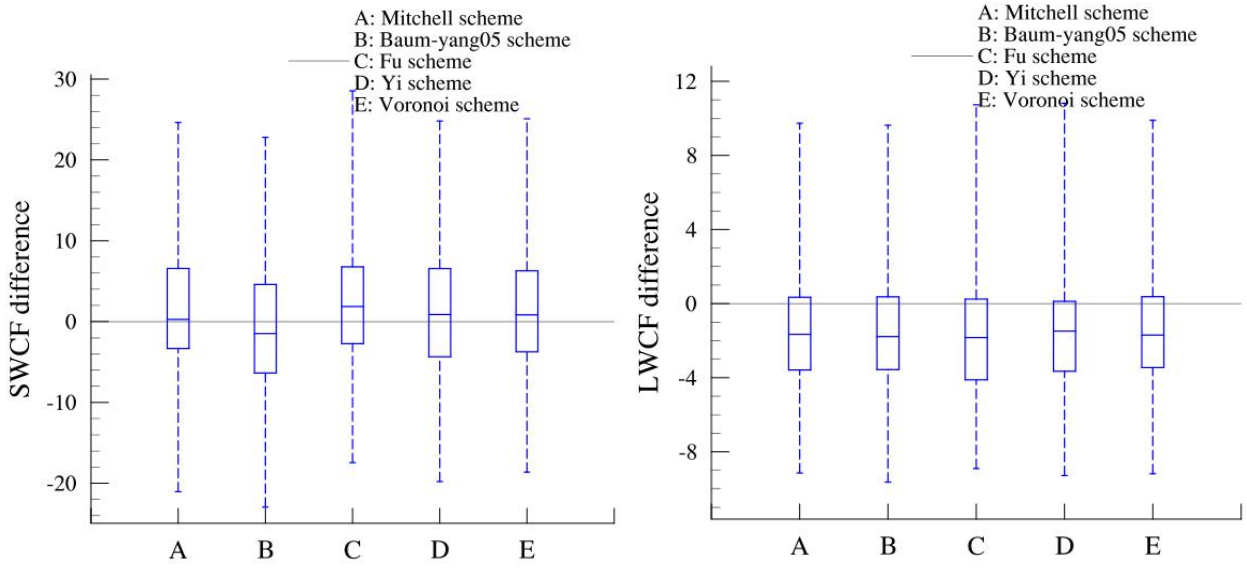

Figure 10. Box analysis of zonal distributions of 10-yr annual mean SWCF (left) and LWCF (right) difference between the Mitchell, Voronoi, Fu, Baum-yang05, Yi scheme and EBAF products, respectively.